Slow Manifold Structure in Explosive Kinetics. 1. Bifurcations of Points-at-Infinity in Prototypical Models

F. Creta,[†] A. Adrover,[‡] S. Cerbelli,[‡] M. Valorani,[†] and M. Giona*[,‡]

Dipartimento di Meccanica e Aeronautica and Dipartimento di Ingegneria Chimica, Facoltà di Ingegneria, Università di Roma "La Sapienza" via Eudossiana 18, 00184 Roma, Italy

Received: June 9, 2006; In Final Form: September 11, 2006

This article analyzes in detail the global geometric properties (structure of the slow and fast manifolds) of prototypical models of explosive kinetics (the Semenov model for thermal explosion and the chain-branching model). The concepts of global or generalized slow manifolds and the notions of heterogeneity and $\alpha-\omega$ inversion for invariant manifolds are introduced in order to classify the different geometric features exhibited by two-dimensional kinetic schemes by varying model parameters and to explain the phenomena that may occur in model reduction practice. This classification stems from the definition of suitable Lyapunov-type numbers and from the analysis of normal-to-tangent stretching rates. In the case of the Semenov model, we show that the existence of a global slow manifold and its properties are controlled by a transcritical bifurcation of the points-at-infinity, which can be readily identified by analyzing the Poincaré projected system. The issue of slow manifold uniqueness and the implications of the theory with regard to the practical definition of explosion limits are thoroughly addressed.

1. Introduction

The mathematical modeling of combustion processes under well-stirred conditions involves the analysis of systems of ordinary differential equations characterized by the occurrence of a broad range of time scales.[1] Time scale heterogeneity implies stiffness (and the ensuing problems in the numerical integration of model equations), but the occurrence of a time scale separation makes it possible to use numerical procedures, algorithms, and computational techniques for solving and reducing the model equations.[2,3] Diagnostic analysis of complex reaction schemes is a central issue in chemical reaction theory and is becoming increasingly important in facing the enormous complexity of biochemical reaction networks associated with subcellular metabolic and regulatory processes.[4,5]

In the search for efficient simplified and reduced models, different computational approaches have been proposed and in some cases successfully applied.[6−11] The geometric paradigm on which all these methods rely is the occurrence of slow invariant manifolds[12−14] within the phase space. Intuitively, slow manifolds are invariant, exponentially attracting manifolds on which neighboring orbits collapse. This implies that, apart for a possibly short transient, the "relevant dynamics" evolves onto a lower-dimensional manifold, along which the original stiffness of the system can be softened, because "fast" modes, which are exhausted, can be removed by projecting them out. Notwithstanding the extensive use of the "slow-manifold paradigm", its definition is somehow still controversial, as witnessed, e.g., by the scientific contest put forward by E. N. Lorenz ("On the nonexistence of a slow manifold"[15] and "The slow manifold—what is it?"[16]) on the existence and meaning of a slow manifold in a low-dimensional model for the shallow water equations.[15−17]

The reason for this and similar controversies in the definition and the meaning of a slow manifold may be attributed to different reasons: (i) the conditions imposed by different authors on slow manifolds may have different natures (e.g., by imposing some smoothness and analyticity criteria on the local representation of the manifold itself[16,17]); (ii) methods and definitions deriving from perturbative analysis of singularly perturbed systems are often intermingled with purely geometric concepts[18] (perturbation studies focus on local portions of a slow manifold near the equilibrium point of a singularly perturbed system, and a purely geometrical definition should be grounded on global properties defined throughout the phase space (see sections 3 and 5)); (iii) in practical applications to model reduction of complex kinetic schemes, "intrinsic low-dimensional manifolds" lack some basic properties (such as invariance), and this collides with more formal mathematical definitions.[19] Correspondingly, the very basic concept of "slow/fast decomposition" of a complex reaction scheme may involve some intrinsic degree of arbitrariness because it relies on the specific method adopted in model diagnostics and reduction (ILDM,[6] CSP,[8] MIM,[20] NTDRB[11]).

Just because of these controversial issues, it is becoming important to attempt to reconcile the various definitions by resorting to a rational geometric characterization of the slow manifold structure, capable of taking into account the different phenomenologies occurring in chemical reaction systems.

The aim of this Article is to address the problem of when and where a dynamical system exhibits a slow manifold and how slow manifolds can be defined and characterized. In this Article, we analyze simple (two-dimensional) models of explosive kinetics, which are especially suited for highlighting the different phenomenologies and "pathologies" associated with the slow manifold structure. The extension to higher dimensional systems is developed in ref 21.

Specifically, we (i) focus on the geometrical problems associated with the existence of slow manifolds and with the

* Corresponding author. E-mail address: max@giona.ing.uniroma1.it.
[†] Dipartimento di Meccanica e Aeronautica.
[‡] Dipartimento di Ingegneria Chimica.

10.1021/jp0636064 CCC: $33.50
Published on Web 11/29/2006

"nonuniformity" of these manifolds and (ii) identify the bifurcational routes that are responsible for the possible "blow-up" of a global slow manifold.

These bifurcations are of local nature and are related to the behavior of the points-at-infinity of the systems. The application of the compactification technique due to Poincaré is the key tool to address "manifold bifurcations". This method has already been applied in the field of complex reaction schemes and manifold structures by Davis and Skodje[22] and by Davis and Klippenstein.[23] The local bifurcations at infinity may have a dramatic impact on the global behavior of the system and can be readily identified by analyzing the Poincaré projected system associated with the original model.

As a model system, we consider the classical Semenov model for a thermal explosion,[24,25] which has been the subject of intense investigation as a benchmark for testing the validity of criteria aimed at determining explosion limits[26−29] and, more recently, for validating some computational methods for model reduction.[18]

We develop a thorough analysis of this model oriented toward the geometric and bifurcational characterization of the slow and fast invariant manifolds. Indeed, the Semenov model provides a simple and clear example of the blow-up of a global slow manifold, which we believe to be frequent in explosive combustion systems. In point of fact, we show that qualitatively similar features (local bifurcation of points-at-infinity and global slow manifold blow-up) occur in other models of combustion kinetics and explosions, such as the chain-branching model.[30]

Although both the Semenov and the chain-branching models can be rightly classified as singularly perturbed problems, we do not analyze these models via classical perturbative methods, but we follow a purely geometric approach, based on the properties of normal/tangent stretching rates, and ultimately on the concept of normal hyperbolicity.[19]

The Article is organized as follows. Section 2 is a concise review of the basic mathematical tools used throughout the Article (e.g., vector dynamics and normal/tangent stretching rates). Section 3 presents a phenomenological overview of the Semenov dynamics as it regards invariant manifold structure and subsequently formulates a geometric definition of global and generalized slow manifolds via the introduction of suitable Lyapunov-type numbers. The development of the theory leads naturally to the introduction of related concepts, namely the $\alpha-\omega$ inversion and the time scale heterogeneity along invariant manifolds. The structure of invariant manifolds can be fruitfully analyzed by introducing the Poincaré projected system associated with the original model. This is presented in section 4 together with the detailed analysis of the local bifurcations of the points-at-infinity for the Semenov model. Compactification methods are also applied to another prototypical model for explosions, the isothermal chain-branching model, for detecting the bifurcations influencing invariant manifold structure. Finally, section 5 addresses some practical issues connected with explosive kinetics and comments on the meaning of the geometric theory developed in the perspective of model simplification and reduction.

2. Basic Definitions and Mathematical Tools

This section introduces the basic definitions and reviews some elementary properties of invariant manifolds.[46]

Consider a generic dynamical system

$$\frac{d\mathbf{z}}{dt} = \mathbf{F}(\mathbf{z}) \tag{1}$$

defined in an n-dimensional phase space, e.g., $\mathbf{z} \in \mathbb{R}^n$, and let $\phi_t(\mathbf{z})$ be the phase flow associated with eq 1. Let $\mathscr{W}$ be an m-dimensional smooth manifold embedded in $\mathbb{R}^n$.[46] The manifold $\mathscr{W}$ is invariant for eq 1 if $\phi_t(\mathbf{z}) \in \mathscr{W}$ for any $\mathbf{z} \in \mathscr{W}$ and for any $t > 0$.

An invariant manifold $\mathscr{W}$ is exponentially attracting for eq 1 if there is a neighborhood U of $\mathscr{W}$ and two positive constants C and λ such that

$$d(\phi_t(\mathbf{z}), \mathscr{W}) \le Ce^{-\lambda t}\, d(\mathbf{z}, \mathscr{W}) \qquad \forall \mathbf{z} \in U \qquad \forall t > 0 \tag{2}$$

where $d(\mathbf{z}, \mathscr{W}) = \inf_{\mathbf{w}\in\mathscr{W}} ||\mathbf{z} - \mathbf{w}||$ is a measure of the minimum distance of point $\mathbf{z}$ from points belonging to the manifold $\mathscr{W}$ and $||\cdot||$ is a norm in $\mathbb{R}^n$ (for example, the Euclidean norm $||\mathbf{z}|| = \sqrt{\sum_{h=1}^{n} z_h^2}$).

Invariance and the exponential attracting nature are the two basic properties defining what is commonly regarded as a slow manifold for eq 1. We will discuss in sections 3 and 5 that these properties should be further complemented by another condition related to the behavior of normal perturbations.

To approach vector dynamics and introduce the definition of linear stability for a one-dimensional invariant manifold (because the properties of one-dimensional invariant manifolds are the main focus of the present Article), let $T_{\mathbf{z}}$ be the tangent space[32] at the point $\mathbf{z}$. $T_{\mathbf{z}}$ is isomorphic to $\mathbb{R}^n$ and can be decomposed into the direct sum $C_{\mathbf{z}} \oplus N_{\mathbf{z}}$, where $C_{\mathbf{z}}$ is the one-dimensional vector subspace spanned by $\mathbf{F}(\mathbf{z})$, i.e., by the vector field itself, and $N_{\mathbf{z}}$ is the orthogonal complement to $C_{\mathbf{z}}$ in $\mathbb{R}^n$. Let $\Pi_{\mathbf{z}}: T_{\mathbf{z}} \to N_{\mathbf{z}}$ be the orthogonal projection operator, mapping a vector $\mathbf{v} \in T_{\mathbf{z}}$ into its component lying in the subspace $N_{\mathbf{z}}$.

Within the tangent bundle, the vector dynamics associated with eq 1 is defined by the linearized equation

$$\frac{d\mathbf{v}(t)}{dt} = \mathbf{F}^*(\mathbf{z}(t))\,\mathbf{v}(t) \qquad \mathbf{v}(t) \in T_{\phi_t(\mathbf{z})} \tag{3}$$

which, when coupled to eq 1, forms a skew-product system,[31] i.e., a system of differential equations, in the present case in the variables $\mathbf{z}$ and $\mathbf{v}$, in which the first set of evolution equations (eq 1) for the variable $\mathbf{z}$ depends exclusively on $\mathbf{z}$ and is decoupled from the evolution equations for $\mathbf{v}$ (eq 3), which depends on both $\mathbf{z}$ and $\mathbf{v}$. In eq 3, $\mathbf{F}^*(\mathbf{z}) = \partial\mathbf{F}(\mathbf{z})/\partial\mathbf{z}$ is the Jacobian matrix of the vector field.

Let $\mathbf{v}(t) = \mathbf{v}(t,\mathbf{z}_0,\mathbf{v}_0)$ be the solution of the skew-product system (eqs 1 and 3) starting from $\mathbf{v}(t=0) = \mathbf{v}_0 \in T_{\mathbf{z}_0}$. The formal solution of eq 3 can be expressed as

$$\mathbf{v}(t) = \mathbf{v}(t,\mathbf{z}_0,\mathbf{v}_0) = \phi_t^*(\mathbf{z}_0)\mathbf{v}_0 \tag{4}$$

where $\phi_t^*(\mathbf{z}) = \partial\phi_t(\mathbf{z})/\partial\mathbf{z}$ is the Jacobian matrix (differential) of the phase flow.

An invariant manifold $\mathscr{W}$ for eq 1 is linearly stable[33] if, for any $\mathbf{z}_0 \in \mathscr{W}$ and $\mathbf{v}_0 \in T_{\mathbf{z}_0}$, the vector $\mathbf{v}(t,\mathbf{z}_0,\mathbf{v}_0)$ satisfies the following inequality:

$$||\Pi_{\phi_t(\mathbf{z}_0)}\mathbf{v}(t,\mathbf{z}_0,\mathbf{v}_0)|| \le C_1 e^{-\lambda_1 t}||\mathbf{v}_0|| \qquad \forall t > 0 \tag{5}$$

for some positive constants C_1 and λ_1.

Equation 5 implies that the normal component of any vector advected by the dynamics eqs 1 and 3 shrinks exponentially in time.

There is a strong relation between exponentially attracting and linearly stable manifolds. Indeed, an invariant manifold for eq 1 is exponentially attracting if and only if it is linearly stable.[34]

The definition of linear stability for invariant manifolds involves vector dynamics, so it is useful to elaborate further for eq 3. By taking the scalar product of both the left- and the right-hand sides of eq 3 with $\mathbf{v}(t)$, one obtains

$$\frac{\mathrm{d}||\mathbf{v}(t)||^2}{\mathrm{d}t} = 2(\mathbf{F}^*\mathbf{v},\mathbf{v}) = 2\,\frac{(\mathbf{F}^*\mathbf{v},\mathbf{v})}{||\mathbf{v}||^2}\,||\mathbf{v}||^2 \tag{6}$$

where $(\mathbf{v},\mathbf{w}) = \Sigma_{h=1}^{n} v_h w_h$ is the scalar product for vectors in $\mathbb{R}^n$. Equation 6 can be formally solved to obtain

$$||\mathbf{v}(t)|| = \mathrm{e}^{\int_0^t (\mathbf{F}^*\hat{\mathbf{v}},\hat{\mathbf{v}})\mathrm{d}\tau}||\mathbf{v}_0|| \qquad \hat{\mathbf{v}} = \mathbf{v}/||\mathbf{v}|| \tag{7}$$

where $\hat{\mathbf{v}}$ is the unit vector spanning $\mathbf{v}$. Equation 7 describes the evolution of vector norms by means of the stretching rate $(\mathbf{F}^*\hat{\mathbf{v}}, \hat{\mathbf{v}})$ where $\mathbf{F}^*$ is the Jacobian matrix of the vector field $\mathbf{F}$ generating the dynamics.

Given a one-dimensional invariant manifold for eq 1, i.e., an orbit for the flow $\phi_t(\mathbf{z})$, two characteristic stretching rates can be defined, associated with the evolution of tangential and normal vectors.

The tangential stretching rate $\omega_\tau(\mathbf{z})$ at points $\mathbf{z} \in \mathscr{W}$ is defined as

$$\omega_\tau(\mathbf{z}) = (\mathbf{F}^*(\mathbf{z})\,\hat{\mathbf{c}}(\mathbf{z}), \hat{\mathbf{c}}(\mathbf{z})) \qquad \mathbf{z} \in \mathscr{W} \tag{8}$$

where $\hat{\mathbf{c}} = \mathbf{F}/||\mathbf{F}||$ is the unit vector tangent to $\mathscr{W}$.

The normal stretching rate $\omega_\nu(\mathbf{z})$ at $\mathbf{z} \in \mathscr{W}$ can be defined as

$$\omega_\nu(\mathbf{z}) = \max_{\hat{\mathbf{n}}\in N_{\mathbf{z}}, ||\hat{\mathbf{n}}||=1} (\mathbf{F}^*(\mathbf{z})\,\hat{\mathbf{n}}(\mathbf{z}), \hat{\mathbf{n}}(\mathbf{z})) \qquad \mathbf{z} \in \mathscr{W} \tag{9}$$

by considering the maximum over all the possible unit vectors $\hat{\mathbf{n}}(\mathbf{z})$ normal to $\mathscr{W}$ at $\mathbf{z}$.

3. Global and Generalized Slow Manifolds

Consider a dynamical system possessing (i) a unique stable equilibrium point $\mathbf{z}_{\mathrm{eq}} = 0$ such that (ii) the linearized dynamics in the neighborhood of $\mathbf{z}_{\mathrm{eq}}$ is characterized by a significant time scale separation in the eigenvalue spectrum. This is a typical situation in which one expects that the slow manifold paradigm would apply; i.e., there must exist a slow invariant attractive manifold $\mathscr{W}$, around which orbit dynamics is organized, so that after a short transient (order of magnitude of the time scales associated with the fast dynamics) orbits collapse onto $\mathscr{W}$. However, this scenario may be more complex in nonlinear systems.

In order to learn from experience the qualitative behavior of the class of systems satisfying the conditions, (i) and (ii), let us first analyze in greater detail the qualitative features of orbit dynamics in the Semenov model, representing the dynamics of a first-order exothermic batch reaction A $\rightarrow$ product in a well-stirred jacketed reactor

$$\frac{\mathrm{d}x}{\mathrm{d}t} = \epsilon^{-1}(yq(x) - x\delta) = \epsilon^{-1}f(x,y)$$

$$\frac{\mathrm{d}y}{\mathrm{d}t} = -yq(x) = g(x,y) \qquad q(x) = \exp(x/(1+\beta x)) \tag{10}$$

We let the model parameters ϵ, β, and δ vary[47] and focus on the different kinds of geometric structures that may appear.

The Semenov model possesses a unique stable equilibrium point $\mathbf{z}_{\mathrm{eq}} = (0, 0)$, and the eigenvalues of the Jacobian matrix $\mathbf{F}^*(\mathbf{z}_{\mathrm{eq}})$ at $\mathbf{z}_{\mathrm{eq}}$ are -1 and $-\epsilon^{-1}\delta$. Provided that $\epsilon^{-1}\delta \gg 1$ (henceforth, we consider exclusively this case), there is a significant time scale separation in the neighborhood of the equilibrium. The eigenspace associated with the slow eigenvalue ($\lambda^s = -1$) is given by $E^s_{\mathbf{z}_{\mathrm{eq}}} = \{\mathbf{v} = (v_1, v_2) | v_2/v_1 = \delta - \epsilon\}$; the fast eigenspace (associated with $\lambda^f = -\epsilon^{-1}\delta$) is given by $E^f_{\mathbf{z}_{\mathrm{eq}}} = \{\mathbf{v} = (v_1, v_2) | v_2 = 0\}$. It is easy to verify that the manifold $\mathscr{W}_x = \{\mathbf{x} | y = 0, x \in [x_c, \infty)\}$ (i.e., the semi-infinite portion of the x-axis starting from $x = x_c = -1/\beta$) is an invariant manifold for the system. Unless otherwise specified, we set $\delta = 1$, because all the characteristic features of the system can be explored by letting the other parameters ϵ and β vary. Moreover, we consider exclusively the case $\epsilon^{-1}\delta > 10$, which corresponds to more than 1 order of magnitude in the time scale separation at equilibrium (0, 0). This implies for the slow eigenspace $E^s_{\mathbf{z}_{\mathrm{eq}}} = \{\mathbf{v} = (v_1, v_2) | v_2/v_1 = \delta - \epsilon = \epsilon(\delta/\epsilon - 1) \simeq \delta = 1\}$, so that it forms an effectively constant angle of about $\pi/4$ with the x-axis for the parameter values considered.

Figure 1A−D depicts the phase-space diagrams (collection of different orbits) for some typical conditions. Panels A and B refer to very small values of ϵ, for two different values of β, i.e., $\beta = 0.31$ (Figure 1A) and $\beta = 0.21$ (Figure 1B), respectively, above and below the characteristic value $\beta^* = 1/4$.[48]

The phase-space diagrams A and B are typical of a nicely behaved system, possessing a global time scale separation between slow and fast dynamical components so that all the different orbits collapse onto a slow manifold (thick line a). This type of slow manifold is an example of what we refer to as a global slow manifold. Throughout this paragraph, we are forced to make an intuitive use of the concepts of "global" and "generalized" slow manifolds that will be introduced and illustrated in the forthcoming sections.

By increasing ϵ, and keeping a significant time scale separation at the equilibrium point, the phase-space diagram changes dramatically. At $\epsilon = 5 \times 10^{-2}$ (Figure 1C,D), it is hard to detect the development of a global slow manifold, because there is an almost uniform distribution of orbits within the phase space, and no global attracting curve can be singled out, even if, close to the origin, a remnant of the finite-length local slow manifold associated with the equilibrium point $\mathscr{W}^s_{\mathbf{z}_{\mathrm{eq}},\mathrm{loc}}$ still persists (Figure 1C). Actually, orbits starting from large values of $y \geq 8$ (Figure 1D) collapse onto the x-axis, which effectively plays the role of a slow manifold, although such direction is associated with the fast eigenspace.

The peculiar features of the phase-space diagrams shown in Figure 1C,D, when compared to those of Figure 1A,B, clearly suggest that, by varying the two controlling parameters β and ϵ, the dynamics undergoes a "bifurcation", causing the blow-up of the "global" slow manifold and the birth of a new kind of invariant structure (which will be referred to as a generalized slow manifold), corresponding, in this case, to the x-axis.

The global slow manifolds depicted in Figure 1 have been obtained by applying the technique of material line advection (MLA), borrowing it from the analysis of chaotic mixing systems.[35,36] The MLA technique for slow manifold identification is briefly reviewed in Appendix A.

Figure 2A,B reviews the geometric structure of the global slow manifolds $\mathscr{W}^s$s for $\beta = 0.31 > \beta^*$ and $\beta = 0.21 < \beta^*$, for several values of ϵ. Specifically, a portion of $\mathscr{W}^s$s close to $\mathbf{z}_{\mathrm{eq}} = (0, 0)$ is depicted.

In both the cases $\beta > \beta^*$ and $\beta < \beta^*$, we observe that, as ϵ increases (following the direction of the arrow in Figure 2A,B), the structure of the global slow manifold changes significantly

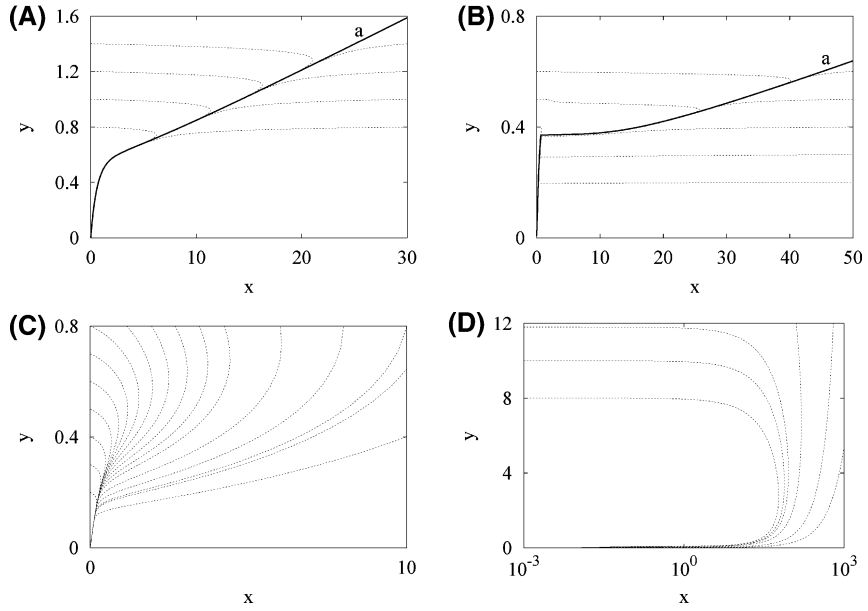

Figure 1. Phase-space diagrams for Semenov model ($\delta = 1$) in several typical cases. Whenever it exists, i.e., in cases A and B, the global slow manifold has been depicted with a thick line (line a in the figures). (A) $\beta > \beta^* = 0.31$, $\epsilon = 10^{-3}$. (B) $\beta < \beta^* = 0.21$, $\epsilon = 10^{-4}$. (C),(D) $\beta = 0.31$, $\epsilon = 5 \times 10^{-2}$.

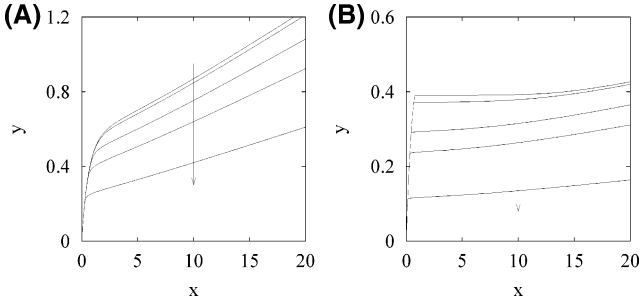

Figure 2. Global slow manifolds of the Semenov model for $\beta = 0.31 > \beta^*$ (A) and $\beta = 0.21 < \beta^*$ (B), for several values of ϵ. (A) $\beta = 0.31$. From top to bottom, in the direction of the arrow: $\epsilon = 10^{-4}$, 10^{-3}, 5×10^{-3}, 10^{-2}, 2×10^{-2}. (B) $\beta = 0.21$. From top to bottom, in the direction of the arrow: $\epsilon = 10^{-5}$, 10^{-4}, 10^{-3}, 2×10^{-3}, 5×10^{-3}.

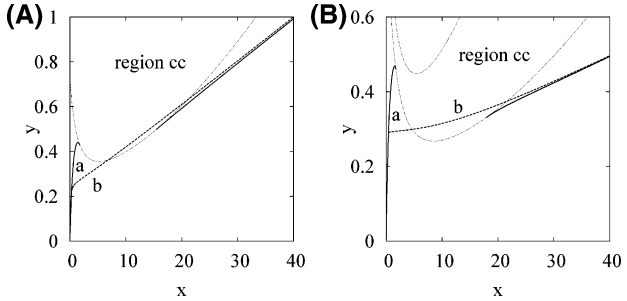

Figure 3. ILDM-approximated manifold (continuous line (a)) and global slow manifold obtained by MLA (dashed curve (b)) of the Semenov model for (A) $\beta = 0.31 > \beta^*$, $\epsilon = 10^{-3}$ and (B) $\beta = 0.21 < \beta^*$, $\epsilon = 2 \times 10^{-3}$. Region cc, bounded by dotted-line curves, is characterized by complex conjugate eigenvalues of the Jacobian matrix.

and seems to collapse onto the *x*-axis. This behavior suggests that, by increasing the value of ϵ (for a fixed value of β), we are getting closer to the bifurcation point at which the global slow manifold blows up and the *x*-axis starts to play the role of a weakly attracting invariant structure (see Figure 1D for $\beta = 0.31$ and $\epsilon = 5 \times 10^{-2}$).

MLA is a very simple and powerful numerical technique for the identification and the computation of one-dimensional slow manifolds, which is based on the idea that a (generalized/global) slow manifold is geometrically represented by the graph of an exponentially attracting, connected, and infinitely extended invariant curve. The infinite extension of the geometric invariant templates is further elaborated in section 4.2 in connection with the role of points-at-infinity and coincides with the analysis presented by Davis and Skodje in ref 22. MLA overcomes all the intrisic limitations of "local" techniques (e.g., ILDM) on the basis of the local eigenvalues/eigenvectors structure, which face significant problems when regions of complex conjugate eigenvalues occur in the phase space.

Consider, for example, in Figure 3A,B, the approximated slow manifold obtained by ILDM (continuous line) and the global slow manifold obtained by MLA (dashed line). The ILDM-approximated slow manifold consists of two disconnected branches separated by the region where complex conjugate eigenvalues appear (region cc, delimited by dotted-line curves). A similar situation occurs in the analysis of the 3-D enzyme inhibition kinetics (EIK) reported in the paper "Global analysis of Enzyme Inhibition Kinetics" by Roussel and Fraser.[37] The authors observe that, for some values of the parameters, it is possible to identify a region in the phase space characterized by a pair of complex conjugate eigenvalues of the Jacobian matrix. Therefore, by making use of local analysis based on the properties of the Jacobian matrix, the authors draw the conclusion that the region of complex eigenvalues (region cc) breaks the 1-D slow manifold into two distinct pieces and that, inside the region of complex conjugate eigenvalues, the 1-D slow manifold is undefined. The analysis of the Semenov model and the technique of MLA reveal that such a conclusion for the EIK model, based exclusively on local analysis, may be erroneous.

Moreover, the left-hand branch, starting from the equilibrium point, results in a nonmonotonic curve, thus violating the invariance property (because, by the nature of the model equation (10), the concentration along any invariant manifold should be a monotonically decreasing function of time, or equivalently, it should be a monotonically increasing function of any curvilinear abscissa *s*, such that $s = 0$ at the equilibrium

point). Further discussion on the ILDM approximation is developed in section 5.

3.1. Global Slow Manifold, $\alpha-\omega$ Inversion and Heterogeneity. The aim of this section is to introduce a geometric definition of global slow manifolds and to present related concepts, namely the phenomenon of $\alpha-\omega$ inversion and the quantification of time scale heterogeneity along invariant manifolds. To simplify the notation, we develop the theory for two-dimensional[6] dynamical systems (as the Semenov model) possessing a unique globally attracting equilibrium point. The extension to higher dimensional systems is developed in full detail in ref 21. The main difference between $n = 2$ and $n > 2$ is that in the latter case the normal subspace $N_{\mathbf{z}}$ at any point $\mathbf{z}$ of the phase space is no longer one-dimensional.

Consider an invariant one-dimensional manifold $\mathscr{W}$(an orbit with starting point z), and let

$$\mathbf{n}_t(\mathbf{z}) = \Pi_{\phi_t(\mathbf{z})}[\phi_t^*(\mathbf{z})\,\mathbf{n}_0] \qquad \mathbf{n}_0 \in N_{\mathbf{z}}$$

$$\mathbf{c}_t(\mathbf{z}) = \phi_t^*(\mathbf{z})\,\mathbf{c}_0 \qquad \mathbf{c}_0 \in C_{\mathbf{z}} \tag{12}$$

Equation 12 expresses the evolution of normal and tangent vectors along the manifold $\mathscr{W}$. Because the normal sub-bundle is not invariant, the normal projector $\Pi_{\phi_t(\mathbf{z})}$ at the image point $\phi_t(\mathbf{z})$ is used in order to obtain the normal component $\mathbf{n}_t(\mathbf{z})$ at the image point. Let us introduce the quantities

$$\Lambda^{\omega} = \lim_{t\to\infty} \frac{\log||\mathbf{n}_t(\mathbf{z})||}{\log||\mathbf{c}_t(\mathbf{z})||} \qquad \mathbf{z} \in \mathscr{W}$$

$$\Lambda^{\alpha} = \lim_{t\to-\infty} \frac{\log||\mathbf{n}_t(\mathbf{z})||}{\log||\mathbf{c}_t(\mathbf{z})||} \qquad \mathbf{z} \in \mathscr{W} \tag{13}$$

The quantities Λ^{α} and Λ^{ω} are referred to as the Lyapunov α- and ω-numbers of the manifold $\mathscr{W}$. The definitions of Λ^{α} and Λ^{ω} adopted here are similar to the definition of the quasi-Lyapunov numbers given by Fenichel.[38] By using the same technique applied by Fenichel,[38] one can prove that Λ^{α} and Λ^{ω} do not depend on the starting point $\mathbf{z} \in \mathscr{W}$ and are intrinsic properties associated with the manifold $\mathscr{W}$.

For dynamical systems possessing a unique asymptotically stable equilibrium point $\mathbf{z}_{\mathrm{eq}}$, it is clear that the behavior for $t \to \infty$ coincides with the behavior of the system in the neighborhood of $\mathbf{z}_{\mathrm{eq}}$, and therefore, the ω-Lyapunov number for any invariant manifold $\mathscr{W}$ can be shown to be expressed as the ratio of the eigenvalues of the Jacobian matrix $\mathbf{F}^*(\mathbf{z}_{\mathrm{eq}})$. In a similar way, the α-Lyapunov number accounts for the normal-to-tangent stretching behavior of a vector at infinity, along the manifold.

In order to show how the α/ω-Lyapunov numbers can be used in defining the properties of the slow manifolds, let us first consider the simple case of a linear two-dimensional autonomous system $\mathrm{d}\mathbf{z}/\mathrm{d}t = A\mathbf{z}$, associated with a constant matrix A, possessing a pair of real and negative eigenvalues $(-\lambda^{\mathrm{s}}, -\lambda^{\mathrm{f}})$, with $\lambda^{\mathrm{s}} < \lambda^{\mathrm{f}}$.

Let E^{s} and E^{f} be the slow and fast eigenspaces associated with the eigenvalues $-\lambda^{\mathrm{s}}$ and $-\lambda^{\mathrm{f}}$, respectively, and spanned by the unit vectors $\mathbf{e}^{\mathrm{s}}$ and $\mathbf{e}^{\mathrm{f}}$. The slow and fast manifolds $\mathscr{W}^{\mathrm{s}}$ and $\mathscr{W}^{\mathrm{f}}$ can be thus defined as $\mathscr{W}^{\mathrm{r}} = \{\mathbf{z}|\mathbf{z} = \xi\mathbf{e}^{\mathrm{r}}, \xi \in (-\infty, \infty)\}$, where $r = \mathrm{s}, \mathrm{f}$. The α/ω-Lyapunov numbers on $\mathscr{W}^{\mathrm{s}}$ and $\mathscr{W}^{\mathrm{f}}$ and on any other invariant manifold $\mathscr{W}$ (which can be viewed as the union of the forward and backward trajectories starting at any point $\mathbf{z}$ not belonging either to $\mathscr{W}^{\mathrm{s}}$ or to $\mathscr{W}^{\mathrm{f}}$) are reviewed[49] in Table 1 (note: it is important to observe that for this class of systems any invariant manifold is also exponentially attracting). The analysis of Table 1 shows that the slow manifold $\mathscr{W}^{\mathrm{s}}$ is characterized by α/ω-Lyapunov numbers both greater than 1. Conversely, the fast manifold is characterized by Lyapunov numbers both strictly smaller than 1; for any other invariant manifold, $\Lambda^{\omega} > 1$ and $\Lambda^{\alpha} < 1$. Indeed, for any $\mathscr{W} \neq \mathscr{W}^{\mathrm{s}}, \mathscr{W}^{\mathrm{f}}$, the scaling for $t \to \infty$ (i.e., close to the equilibrium $\mathbf{z}_{\mathrm{eq}}$) of tangential vector norms is controlled by λ^{s}, and the normal vectors decay as $\mathrm{e}^{-\lambda^{\mathrm{f}}t}$; for $t \to -\infty$, tangential vectors grow as $\mathrm{e}^{-\lambda^{\mathrm{f}}t}$ and normal vectors as $\mathrm{e}^{-\lambda^{\mathrm{s}}t}$.

TABLE 1: α/ω-Lyapunov Numbers along the Invariant Manifolds of a Linear Autonomous Two-Dimensional System

manifold	Λ^{ω}	Λ^{α}
$\mathscr{W}^{\mathrm{s}}$	$\lambda^{\mathrm{f}}/\lambda^{\mathrm{s}} > 1$	$\lambda^{\mathrm{f}}/\lambda^{\mathrm{s}} > 1$
$\mathscr{W}^{\mathrm{f}}$	$\lambda^{\mathrm{s}}/\lambda^{\mathrm{f}} < 1$	$\lambda^{\mathrm{s}}/\lambda^{\mathrm{f}} < 1$
$\mathscr{W}$	$\lambda^{\mathrm{f}}/\lambda^{\mathrm{s}} > 1$	$\lambda^{\mathrm{s}}/\lambda^{\mathrm{f}} < 1$

Therefore, the slow invariant manifold $\mathscr{W}^{\mathrm{s}}$ can be discriminated from all the other invariant manifolds $\mathscr{W}^{\mathrm{f}}$ or $\mathscr{W}$ for its peculiar behavior for $t \to -\infty$, as it is the unique invariant manifold for which $\Lambda^{\alpha} > 1$, whereas the fast manifold $\mathscr{W}^{\mathrm{f}}$ is the only invariant manifold for which $\Lambda^{\omega} < 1$.

This result can be readily extended to a nonlinear system (eq 1) possessing a unique globally attracting equilibrium point $\mathbf{z}_{\mathrm{eq}}$ (henceforth, we will consider exclusively this case, and therefore, this specification will be omitted). In the extension to nonlinear systems, it is convenient to view any one-dimensional invariant manifold as a curve possessing the equilibrium point $\mathbf{z}_{\mathrm{eq}}$ as one of its endpoints. Therefore, the slow manifold $\mathscr{W}^{\mathrm{s}}$ defined for the linear system considered above could be viewed as the union of two distinct slow manifolds $\mathscr{W}_1^{\mathrm{s}} = \{\mathbf{z}|\mathbf{z} = \xi\mathbf{e}^{\mathrm{s}}, \xi \in [0, \infty)\}$, $\mathscr{W}_2^{\mathrm{s}} = \{\mathbf{z}|\mathbf{z} = \xi\mathbf{e}^{\mathrm{s}}, \xi \in (-\infty, 0]\}$. Although this distinction seems rather artificial for linear systems, it is a convenient one for a proper definition of slow manifolds in nonlinear dynamics.

We are now able to formalize the geometric definitions for slow/fast manifolds and global slow/fast manifolds.

Given the dynamical system eq 1, a global 1-D slow manifold is an invariant, exponentially attracting (i.e., linearly stable) one-dimensional manifold for which $\Lambda^{\alpha} > 1$ and $\Lambda^{\omega} > 1$. A global 1-D fast manifold is an invariant, exponentially attracting one-dimensional manifold for which $\Lambda^{\alpha} < 1$ and $\Lambda^{\omega} < 1$.

From the analysis of linear systems, we know that the peculiar feature of a slow manifold is essentially the vector scaling for $t \to -\infty$ (quantified by the α-Lyapunov number $\Lambda^{\alpha} > 1$) and a fast manifold is characterized by the vector scaling for $t \to \infty$ (quantified by the ω-Lyapunov number $\Lambda^{\omega} < 1$).

For this reason, it is convenient to give another, weaker definition of slow/fast manifolds, exclusively based on their asymptotic backward/forward behavior in time.

Given the dynamical system eq 1, a generalized 1-D slow manifold is an invariant, exponentially attracting one-dimensional manifold for which $\Lambda^{\alpha} > 1$. A generalized 1-D fast manifold is an invariant, exponentially attracting one-dimensional manifold for which $\Lambda^{\omega} < 1$.

Obviously, a global slow (fast) manifold is *a fortiori* a generalized slow (fast) manifold, but the opposite does not hold. For example, let us consider a generalized slow manifold $\mathscr{W}$ and suppose that $\Lambda^{\omega} < 1$. This means that the dynamics along $\mathscr{W}$ in the neighborhood of $\mathbf{z}_{\mathrm{eq}}$ behaves as on a local fast manifold. Actually, in this case, the invariant manifold $\mathscr{W}$ is a generalized slow manifold and a generalized fast manifold, at the same time. We refer to this particular situation as an $\alpha-\omega$ inversion. The $\alpha-\omega$ inversion cannot occur in linear systems but is frequent in nonlinear models, in association with local bifurcations at the points-at-infinity (see section 4).

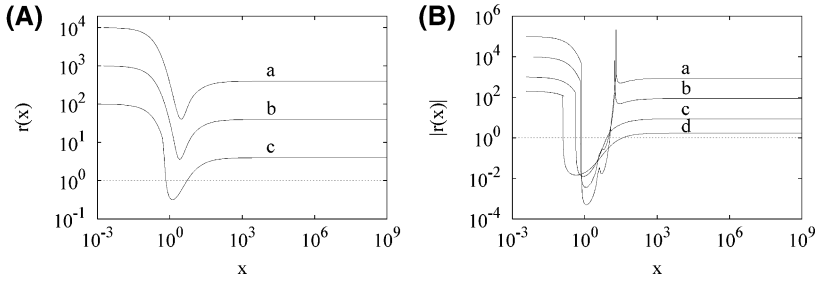

Figure 4. Stretching ratio $r(x)$ vs x along the global slow manifolds. (A) $\beta = 0.31 > \beta^*$. Line a refers to $\epsilon = 10^{-4}$, line b to $\epsilon = 10^{-3}$, and line c to $\epsilon = 10^{-2}$. (B) $\beta = 0.21 < \beta^*$. This figure depicts the absolute value of $r(x)$, because the tangential stretching rate may attain both negative and positive values. Line a refers to $\epsilon = 10^{-5}$, line b to $\epsilon = 10^{-4}$, line c to $\epsilon = 10^{-3}$, line d to $\epsilon = 5 \times 10^{-3}$. The dotted line indicates $r = 1$.

The phenomenon of $\alpha-\omega$-inversion for a generalized slow manifold can be easily understood by analyzing the local properties in the evolution of normal and tangential vectors along the manifold. This can be done by introducing the pointwise stretching ratio $r(\mathbf{z})$

$$r(\mathbf{z}) = \frac{\omega_\nu(\mathbf{z})}{\omega_\tau(\mathbf{z})} \tag{14}$$

The case $\omega_\nu(\mathbf{z}) > 0$ is not relevant to our analysis, because we are always assuming that $\mathscr{W}$ is an exponentially attracting manifold. If $r(\mathbf{z}) > 1$ and $\omega_\tau(\mathbf{z}) < 0$, normal vectors shrink at $\mathbf{z}$ faster than tangential vectors. Conversely, if $r(\mathbf{z}) < 1$ and $\omega_\tau(\mathbf{z}) < 0$, vector dynamics tangent to the manifold is faster than normal vector shrinking. If $r(\mathbf{z}) < 0$, then $\omega_\tau(\mathbf{z}) > 0$; that is, tangential vectors stretch exponentially and normal vectors contract. Different diagrams illustrating the behavior of the pointwise stretching ratio $r(\mathbf{x})$ and the occurrence of $\alpha-\omega$ inversion for the Semenov model are reported in section 3.2 (see Figure 4A,B).

For generic nonlinear systems, a generalized (or global) one-dimensional slow manifold $\mathscr{W}$ is heterogeneous if $r(\mathbf{z})$ is not constant for $\mathbf{z} \in \mathscr{W}$. A generalized (or global) one-dimensional slow manifold $\mathscr{W}$ is inverting if there is a point $\mathbf{z}^* \in \mathscr{W}$ and an open neighborhood $U_{\mathbf{z}}^*$ of $\mathbf{z}^*$, such that $r(\mathbf{z}) < 1$ for $\mathbf{z} \in \mathscr{W} \cap U_{\mathbf{z}^*}$.

From the physical point of view, the occurrence of inversion, i.e., the existence within a global slow manifold $\mathscr{W}$ of regions where $r(\mathbf{z}) < 1$, is the indicator of some local "pathology" in the dynamical behavior of the system near $\mathscr{W}$. Namely, although $\mathscr{W}$ is globally attracting, there are portions of $\mathscr{W}$ (the inverting regions) in which nearby orbits to the manifold are almost neutrally attracted; i.e., they are practically parallel to the slow manifold itself. This is a consequence of the fact that normal perturbations decay more slowly than tangential ones, and the overall phase-space structure within an inverting region appears as a bundle of parallel orbits to the slow manifold. This situation is clearly depicted in Figures 1B and 2B. The occurrence of inversion has significant implications in model reduction, as discussed in section 5.2, and this represents the main motivation for the introduction of this concept.

By definition, a generalized slow manifold, for which $\Lambda^\omega < 1$, is inverting, because $r(\mathbf{z}) < 1$ in the neighborhood of $\mathbf{z}_{\text{eq}}$. However, even a global slow manifold $\mathscr{W}$ may be inverting at points other than $\mathbf{z}_{\text{eq}}$. The occurrence of inversion influences the global dynamics around $\mathscr{W}$. In the next section, we apply the concepts introduced above to the analysis of slow/fast manifolds of the Semenov model.

3.2. Slow/Fast Manifolds, $\alpha-\omega$ Inversion, and Heterogeneity in the Semenov Model. Let us consider the Semenov model. For this system, the manifold $\mathscr{W}_x^+ = \{\mathbf{z} | y = 0, x \geq 0\}$ is an invariant manifold characterized by tangential and normal stretching rates $\omega_\tau(x) = -\epsilon^{-1}\delta$ and $\omega_\nu(x) = -q(x)$, respectively. Because $\omega_\nu(x) < 0$ at each point of the manifold, $\mathscr{W}_x^+$ is linearly stable (i.e., exponentially attracting). Moreover, it is characterized by the following α/ω-Lyapunov number

$$\Lambda^\omega = \frac{-q(0)}{-\epsilon^{-1}\delta} = \frac{1}{\epsilon^{-1}\delta} < 1 \tag{15}$$

$$\Lambda^\alpha = \frac{-q(\infty)}{-\epsilon^{-1}\delta} = \frac{e^{1/\beta}}{\epsilon^{-1}\delta} = \begin{cases} >1 \text{ for } \epsilon > \delta e^{-1/\beta} \\ <1 \text{ for } \epsilon > \delta e^{-1/\beta} \end{cases} \tag{16}$$

Therefore, there exists a critical value of ϵ, namely $\epsilon_c(\delta,\beta)$ defined as

$$\epsilon_c(\delta,\beta) = \delta e^{-1/\beta} \tag{17}$$

3.2.1. Discussion for $\epsilon < \epsilon_c$. For $\epsilon < \epsilon_c$, the manifold $\mathscr{W}_x^+$ is a global fast manifold because both $\Lambda^\omega < 1$ and $\Lambda^\alpha < 1$ hold. Moreover, for $\epsilon < \epsilon_c$ at each point on the manifold, $\omega_\tau < 0$ and $r(x) = q(x)/(\epsilon^{-1}\delta) \leq q(\infty)/(\epsilon^{-1}\delta) = e^{1/\beta}/(\epsilon^{-1}\delta) < 1$; i.e., tangential vectors shrink faster than normal vectors and the global fast manifold is noninverting.

This case corresponds to the phase-space diagrams reported in Figure 1A,B, showing the existence of a monotonic global slow manifold $\mathscr{W}_1^s$ for both cases $\beta > \beta^*$ (Figure 1A) and $\beta < \beta^*$ (Figure 1B). Similarly, all the global slow manifolds shown in Figure 2A ($\beta > \beta^*$) and Figure 2B ($\beta < \beta^*$) correspond to values of ϵ and β such that $\epsilon < \epsilon_c(\delta,\beta)$.

The dynamical properties along the global slow manifold for $\epsilon < \epsilon_c$ are depicted in Figure 4A,B for values of β above and below the critical value $\beta^* = 1/4$.

Figure 4A shows the stretching rate $r(x)$ vs x along the global slow manifold $\mathscr{W}_1^s$ (computed by MLA) for $\beta = 0.31 > \beta^*$ and several values of $\epsilon < \epsilon_c$. We first observe from eqs 15 and 16 that (i) for $x \to \infty$, $r(x) \to \Lambda^\alpha > 1$ and for $x \to 0$, $r(x) \to \Lambda^\omega > 1$, so that the invariant manifolds are global slow manifolds, and (ii) the α-Lyapunov number decreases for increasing values of ϵ in such a way that $\Lambda^\alpha \to 1$ for $\epsilon \to \epsilon_c$ (for $\delta = 1$, $\beta = 0.31$, the critical value of ϵ is $\epsilon_c = 3.97 \times 10^{-2}$). Moreover, for very small values of ϵ, the global slow manifold is noninverting (curve a and b in Figure 4A); for $\epsilon = 10^{-2}$, there exists an intermediate region along the manifold at which $r(x) < 1$ (inversion).

A similar situation occurs for $\beta = 0.21 < \beta^*$ and $\epsilon < \epsilon_c$, as depicted in Figure 4B—in this case, the critical value is $\epsilon_c = 8.55 \times 10^{-3}$—although the dynamical picture of vector-norm dynamics along the global slow manifold is slightly more complex. First, inversion occurs for any value of $\epsilon < \epsilon_c$. Moreover, curves a and b, corresponding to $\epsilon = 10^{-5}$ and 10^{-4},

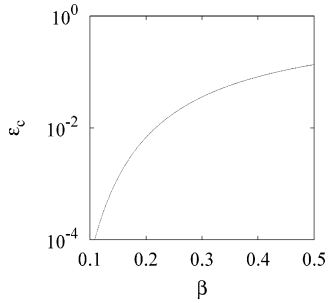

Figure 5. Log−normal plot of ϵ_c as a function of β for $\delta = 1$.

respectively, show the occurrence of positive tangential stretching rates along the global slow manifold $\mathscr{W}_1^s$.

3.2.2. Discussion for $\epsilon > \epsilon_c$. For $\epsilon > \epsilon_c(\delta,\beta)$, the manifold $\mathscr{W}_x^+$ is a generalized slow manifold ($\Lambda^\alpha > 1$) exhibiting $\alpha-\omega$ inversion (because $\Lambda^\omega < 1$) and is inverting in the interval $[0, x^*)$, $x^* = \log(\epsilon^{-1}\delta)/(1 - \beta \log(\epsilon^{-1}\delta))$ because $r(x) < 1$ for $x \in [0, x^*)$ and $r(x) > 1$ for $x \in (x^*, \infty)$. This case corresponds to the phase-space diagrams reported in Figure 1C,D, showing the blow-up of the global slow manifold and the birth of the generalized slow manifold $\mathscr{W}_x^+$ that, close to the equilibrium point $\mathbf{z}_{eq}$, is tangent to the fast eigendirection.

Therefore, we conclude that the basic criterion to distinguish between the two completely different dynamical behaviors of the Semenov system exhibited in Figure 1A,B and Figure 1C,D is based on the comparison between ϵ (for fixed values of δ and β) and the critical value $\epsilon_c(\delta,\beta)$. The behavior of ϵ_c as a function of β for $\delta = 1$ is reported in Figure 5.

In the next section, by making use of the Poincaré projected system, we show that the existence of global (or generalized) slow manifolds and their properties are controlled by a transcritical bifurcation of the point-at-infinity occurring at $\epsilon = \epsilon_c(\delta,\beta)$.

4. Poincaré Projected System and Bifurcations of Points-at-Infinity

A (generalized/global) slow manifold is geometrically represented by the graph of an exponentially attracting, connected, and infinitely extended invariant curve characterized by ω- and α-Lyapunov numbers greater than one. The α-Lyapunov number accounts for the normal-to-tangent stretching behavior of a vector at infinity, i.e., far from the equilibrium point, along the manifold. In order to investigate this behavior at infinity, it is extremely useful to make use of a compactification[39] of the phase space, i.e., the one-to-one mapping of the phase space onto a compact domain.

The idea of analyzing the global behavior of a planar dynamical system by using a stereographic projection of the sphere onto the plane is due to Bendixson.[40] A more convenient approach for studying the behavior of trajectories "at infinity" is to use the so-called Poincaré sphere, where we project from the center of the unit sphere ($\mathcal{S}^2 = \{(X, Y, Z) \in \mathbb{R}^3 | X^2 + Y^2 + Z^2 = 1\}$) onto the (x, y) plane, tangent to $\mathcal{S}^2$ at either the north or the south pole. This type of central projection has the advantage that the critical points-at-infinity are spread out along the equator of the Poincaré sphere.

Therefore, the structure and properties of invariant manifolds can be further addressed by introducing the Poincaré projected system[22,40] associated with eq 1, by defining the following coordinate transformation (throughout this section, we consider two-dimensional systems):

$$u_h = \frac{z_h}{\sqrt{1 + \sum_{k=1}^{2} z_k^2}} \qquad h = 1, 2 \tag{18}$$

, which is a homeomorphism, the inverse transformation of which is given by $z_h = u_h/[1 - \Sigma_{k=1}^2 u_k^2]^{1/2}$, $h = 1, 2$.

Under this coordinate change, $\mathbb{R}^2$ is mapped onto the two-dimensional unit sphere $\mathcal{S}_2 = \{\mathbf{u} = (u_1, u_2) | u_1^2 + u_2^2 \le 1\}$, and the behavior on the boundary $\partial\mathcal{S}_2^1 = \{\mathbf{u} | u_1^2 + u_2^2 = 1\}$ corresponds to the behavior at infinity for eq 1.

Let F_1 and F_2 be the entries of the vector field $\mathbf{F}$ associated with eq 1. The Poincaré projected system associated with eq 1 is given by

$$\frac{du_h}{dt} = (1 - \sum_{k=1}^{2} u_k^2)^{1/2}[F_h - u_h \sum_{k=1}^{2} u_k F_k] \qquad h = 1, 2 \tag{19}$$

The introduction of the Poincaré projected system eq 19 (henceforth indicated as Pp-system, for short) permits the analysis of the global behavior of eq 1 in terms of the properties of the equilibrium points-at-infinity. In fact, let us consider an autonomous linear system $d\mathbf{z}/dt = A\mathbf{z}$ where the matrix A possesses two real and distinct eigenvalues, the unit eigenvectors of which are $\mathbf{e}_h$ ($||\mathbf{e}_h|| = 1$), $h = 1, 2$. Elementary algebraic manipulations show that the Pp-system possesses five equilibrium points: (i) the equilibrium point $\mathbf{u}_{eq} = 0 = (0, 0)$ corresponding to the unique equilibrium point $\mathbf{z}_{eq} = 0$ of the original system and (ii) four equilibrium points-at-infinity $\mathbf{u}_{eq}^{\infty,\pm} = \pm\mathbf{e}_h$, $h = 1, 2$. Therefore, the equilibrium points-at-infinity correspond to the invariant directions associated with the one-dimensional eigenmanifolds of the system. This observation can be extended to nonlinear systems and leads to a simple geometric definition of global/generalized slow/fast manifolds.

For a dynamical system possessing a unique globally attracting equilibrium point $\mathbf{z}_{eq} = 0$, global/generalized one-dimensional invariant manifolds are the heteroclinic orbits of the Pp-system connecting $\mathbf{u}_{eq} = 0$ to equilibrium points-at-infinity $\mathbf{u}_{eq}^{\infty}$, such that the α/ω-Lyapunov numbers Λ^ω and Λ^α possess prescribed (and specific) properties (as discussed in section 3.1). This is the geometric picture discussed by Davis and Skodje.[22]

The concept of the global/generalized invariant manifolds as heteroclinic orbits connecting $\mathbf{z}_{eq}$ to a point-at-infinity permits a unified view of the α/ω-Lyapunov numbers, defined in section 3.1. Indeed, as Λ^ω expresses the local scaling of the normal-to-tangent vector norms along a given manifold $\mathscr{W}$ in the neighborhood of $\mathbf{z}_{eq}$, the α-Lyapunov number Λ^α accounts for the local scaling of the same quantity in the neighborhood of the point-at-infinity along the heteroclinic connection.

4.1. Bifurcations and Manifold Structure in the Semenov Model. The introduction of the Pp-system allows us to address the global qualitative properties of the Semenov model and its global changes in the invariant manifold structure viewed as local bifurcations associated with the points-at-infinity. This approach is particularly simple for the Semenov model as for $x \to \infty$, $q(x) \to e^{1/\beta}$, and therefore, the behavior at infinity is described by the linear system $d\mathbf{z}/dt = \mathbf{A}_\infty\mathbf{z}$, where

$$\mathbf{A}_\infty = \begin{pmatrix} -\epsilon^{-1}\delta & \epsilon^{-1}e^{1/\beta} \\ 0 & -e^{1/\beta} \end{pmatrix} \tag{20}$$

The matrix $\mathbf{A}_\infty$ admits as eigenvalues $\lambda_1^\infty = -\epsilon^{-1}\delta$ and $\lambda_2^\infty = -e^{1/\beta}$, the eigenvectors of which are $\mathbf{e}_1^\infty = (1, 0)$ and $\mathbf{e}_2^\infty = (C,$

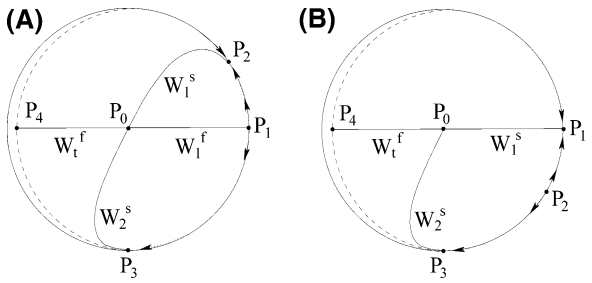

Figure 6. Pictorial representation of the points-at-infinity, their stability, and the structure of slow and fast manifolds for the Semenov model: (A) $\epsilon < \epsilon_c$; (B) $\epsilon > \epsilon_c$. The dashed line shows the boundary of the admissible phase space $x = x_c = -1/\beta$. Points P_1 and P_2 correspond to the equilibrium points-at-infinity $\mathbf{u}^{\infty}_{eq,1}$ (or θ^*_1) and $\mathbf{u}^{\infty}_{eq,2}$ (or θ^*_2), respectively. The point $(x_c, 0)$ in the x,y-plane is represented by the point P_4 on $\partial\mathcal{J}^1_2$.

C ($e^{-1/\beta}\delta - \epsilon$)), respectively, where C is a normalization constant $C = [1 + (e^{-1/\beta}\delta - \epsilon)^2]^{-1/2}$. The equilibrium points-at-infinity of the Pp-system are associated with the eigendirections of $\mathbf{A}_\infty$. It follows that the Pp-system admits two equilibrium points-at-infinity, $\mathbf{u}^{\infty}_{eq,1} = \mathbf{e}^{\infty}_1$ and $\mathbf{u}^{\infty}_{eq,2} = \mathbf{e}^{\infty}_2$ within the semicircle $u_1 > 0$.

The point $\mathbf{u}_{eq} = 0$ is globally attracting, and the two points-at-infinity $\mathbf{u}^{\infty}_{eq,1}$ and $\mathbf{u}^{\infty}_{eq,2}$ are unstable for the Pp-system defined on the Poincaré circle $\mathcal{J}_2$. They are either saddles or unstable sources. To decide it, consider the dynamics of the Pp-system restricted to the equator of the Poincaré sphere, i.e., on the boundary $\partial\mathcal{J}^1_2 = \{(u_1, u_2)|u_1^2 + u_2^2 = 1\}$, which is an invariant set for the Pp-system and along which $u_1 = \cos\theta$, $u_2 = \sin\theta$, $\theta \in [0, 2\pi]$.

By enforcing eq 19, it follows that the dynamics in the angular variable θ on $\partial\mathcal{J}^1_2$ satisfies the equation

$$\frac{d\theta}{dt} = \frac{u_1\dot{u}_2 - u_2\dot{u}_1}{u_1^2 + u_2^2} = A_{21}u_1^2 - A_{12}u_2^2 + (A_{22} - A_{11})u_1u_2 \tag{21}$$

where $\dot{u}_h = du_h/dt$. The substitution in eq 21 of the expression for $\mathbf{A} = \mathbf{A}_\infty$ eq 20, deriving from the behavior at infinity of the Semenov model, yields

$$\frac{d\theta}{dt} = G(\theta) = -\epsilon^{-1}e^{1/\beta}\sin^2\theta + (\epsilon^{-1}\delta - e^{1/\beta})\sin\theta\cos\theta \tag{22}$$

From eq 22, it follows that there are two equilibrium points, $\theta^*_1 = 0$ (associated with $\mathbf{u}^{\infty}_{eq,1}$) and $\theta^*_2 = \arctan(e^{-1/\beta}\delta - \epsilon)$ (associated with $\mathbf{u}^{\infty}_{eq,2}$).

For $\epsilon < \epsilon_c = e^{-1/\beta}\delta$, θ^*_1 is unstable; $\theta^*_2 > 0$ is stable on $\partial\mathcal{J}^1_2$. For $\epsilon > \epsilon_c$, θ^*_2 moves into the fourth quadrant and loses stability, and θ^*_1 becomes stable, as depicted in Figure 6.

Therefore, the analysis of the Pp-system restricted to the equator of the Poincaré sphere eq 22 clearly shows that, for $\epsilon = \epsilon_c$, a transcritical bifurcation[41] occurs at infinity in the Semenov model, corresponding to the exchange of stability between the two equilibrium points-at-infinity, θ^*_1 (associated with $\mathbf{u}^{\infty}_{eq,1}$) and θ^*_2 (associated with $\mathbf{u}^{\infty}_{eq,2}$). The bifurcation diagram for $\beta = 0.21$ and $\delta = 1$ is reported in Figure 7. Actually, the bifurcation locus in the parameter space is expressed by the equation

$$b(\delta,\beta,\epsilon) = e^{-1/\beta}\delta - \epsilon = 0 \tag{23}$$

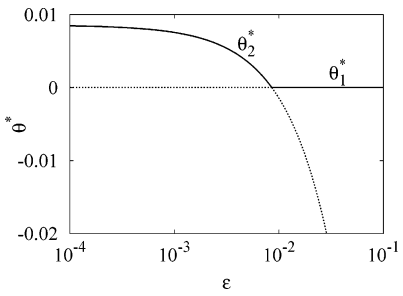

Figure 7. Transcritical bifurcation occurring in the Semenov model at the point-at-infinity ($\beta = 0.21$, $\delta = 1$), by considering ϵ as a parameter. Solid lines are the stable branches, dotted lines the unstable branches.

and, by considering ϵ as the bifurcation parameter, we find that the transcritical bifurcation occurs at $\epsilon = \epsilon_c = e^{-1/\beta}\delta$, in agreement with eq 17.

The transcritical bifurcation at infinity controls the structure of the slow invariant manifolds and is responsible for the blow-up of the global slow manifold in the first quadrant of the x,y-plane, already observed in section 3.

Indeed, for $\epsilon < \epsilon_c$, the point-at-infinity $\mathbf{u}^{\infty}_{eq,2}$ is a saddle and is attracting on $\partial\mathcal{J}^1_2$. This means that any infinitely long material line (in the Pp-system, this corresponds simply to a material line connecting $\mathbf{u}_{eq} = 0$ to a generic point on $\partial\mathcal{J}^1_2$, with $u_1 > 0$) is attracted toward the global slow manifold represented by the invariant heteroclinic orbit connecting $\mathbf{u}_{eq}$ to $\mathbf{u}^{\infty}_{eq,2}$ (curve $\mathcal{W}^s_1$ connecting P_0 and P_2 in Figure 6A). Conversely, the x-axis (or, more precisely, the non-negative portion of the x-axis, corresponding to the manifold $\mathcal{W}^f_1$ in Figure 6A connecting P_0 and P_1) is a global fast manifold of the system, connecting $\mathbf{u}_{eq}$ to the unstable point-at-infinity $\mathbf{u}^{\infty}_{eq,1}$. The dynamical properties along the global slow and fast manifolds for $\epsilon < \epsilon_c$ have been analyzed in detail in section 3.1 (Figure 4A,B).

For $\epsilon > \epsilon_c$, the global structure of the invariant manifolds changes dramatically. The global slow manifold blows up, because at infinity $\mathbf{u}^{\infty}_{eq,2}$ moves into the fourth quadrant and becomes unstable, and correspondingly, $\mathbf{u}^{\infty}_{eq,1}$ becomes stable on $\partial\mathcal{J}^1_2$ after the transcritical bifurcation.

The exchange of stability between $\mathbf{u}^{\infty}_{eq,1}$ and $\mathbf{u}^{\infty}_{eq,2}$ corresponds to an exchange of stability between the global slow manifold $\mathcal{W}^s_1$ (defined for $\epsilon < \epsilon_c$) and $\mathcal{W}^f_1$. Indeed, for $\epsilon > \epsilon_c$, $\mathbf{u}^{\infty}_{eq,1}$ is a saddle and is attracting on $\partial\mathcal{J}^1_2$ and the positive part of the x-axis is a heteroclinic orbit connecting $\mathbf{u}_{eq}$ to the point-at-infinity $\mathbf{u}^{\infty}_{eq,1}$ characterized by the Lyapunov-numbers $\Lambda^\omega < 1$ and $\Lambda^\alpha > 1$. Therefore, for $\epsilon > \epsilon_c$, it behaves as the unique generalized slow manifold defined in the physically admissible region of the phase space.

Figure 8A,B shows the manifold structures for the Semenov model on the Poincaré circle for $\beta = 0.21$, $\delta = 1$, $\epsilon = 10^{-4} < \epsilon_c$ (Figure A), and $\epsilon = 10^{-2} > \epsilon_c$ (Figure B). Although very close to P_1, the point P_2 (corresponding to $\mathbf{u}^{\infty}_{eq,2}$) is indeed different from P_1. Global and generalized slow manifolds are obtained by the MLA technique.

For the sake of completeness, Figure 8A,B also shows the behavior of the heteroclinic orbit $\mathcal{W}^s_2$ connecting $\mathbf{u}_{eq}$ (point P_0) to the point-at-infinity $P_3 = (0, -1)$ (corresponding to the point $(x_c, -\infty)$ in the x,y-plane) and representing the unique global slow manifold in the nonphysically admissible region (negative reactant concentrations) of the phase space.

The blow-up of a global slow manifold for $\epsilon > \epsilon_c$ makes particularly evident the occurrence of finite-length slow manifolds associated with the local behavior of the system close to

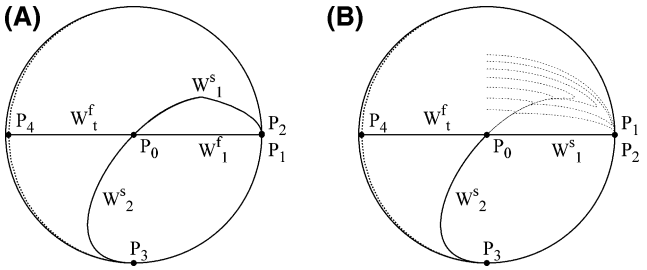

Figure 8. Manifold structure of the Semenov model ($\beta = 0.21$, $\delta = 1$) on the Poincaré circle: (A) $\epsilon = 10^{-4}$; (B) $\epsilon = 10^{-2}$. The thicker dotted line in the second and third quadrants is the boundary of the phase space $x_c = -1/\beta$. The dotted lines depict typical orbits.

$\mathbf{z}_{eq}$. This phenomenon can be appreciated by analyzing the phase-space diagram in the x,y-plane reported in Figure 1C ($\beta = 0.31$, $\epsilon = 5 \times 10^{-2} > \epsilon_c$) as well as the different orbits in the first quadrant of the Poincaré circle obtained from the numerical integration of the Pp-system associated to the Semenov model for $\beta = 0.21$ and $\epsilon = 10^{-2} > \epsilon_c$ (see Figure 8B). The classification of these finite-length slow manifolds is addressed in the next subsection.

4.2. Transient and Hartman−Grobman Slow Manifolds. The definition of slow/fast manifolds as heteroclinic orbits connecting $\mathbf{z}_{eq}$ to equilibrium points-at-infinity is still not exhaustive, and a further categorization is needed to account for what can occur in nonlinear systems. To show this, consider again the Semenov model.

This model possesses the characteristic property that the phase space does not coincide with $\mathbb{R}^2$, because the half-plane to the left of $x_c = -1/\beta$ corresponds to negative temperatures. The admissible phase space is therefore a domain of $\mathbb{R}^2$ with boundary.

The invariant manifold $\mathscr{W}_x = \{\mathbf{z}|y = 0, x \in [x_c, \infty)\}$ splits into two distinct submanifolds (see Figure 8): a heteroclinic orbit connecting points P_0 and P_1 (representing a global fast manifold $\mathscr{W}_1^f = \mathscr{W}_x^+$ for $\epsilon < \epsilon_c$ and a generalized slow manifold $\mathscr{W}_1^s$ for $\epsilon > \epsilon_c$) and the "finite-length" fast manifold $\mathscr{W}_t^f = \{(x, y)|y = 0, x \in [-1/\beta, 0]\}$ connecting P_0 to the point on the boundary P_4. The occurrence of the finite-length manifold $\mathscr{W}_t^f$ in the Semenov model leads to the definition of proper and transient slow/fast manifolds.

A proper (global or generalized) slow manifold is geometrically represented by the graph of an exponentially attracting, connected, and infinitely extended invariant curve. It represents the invariant exponentially attracting heteroclinic connection between the equilibrium point $\mathbf{z}_{eq}$ and a point-at-infinity for which $\Lambda^\alpha > 1$ ($\Lambda^\omega < 1$ for fast manifolds). In the case of a proper global slow (fast) manifold, the further condition $\Lambda^\omega > 1$ ($\Lambda^\alpha < 1$ for fast manifolds) holds. Invariance and infinite extension imply that a proper invariant manifold is actually properly invariant; i.e., the image of the manifold through the phase flow concides with the manifold itself, $\phi_t(\mathscr{W}) = \mathscr{W}$ for any t. Moreover, the definition of proper manifolds as heteroclinic connections between the equilibrium point, and a given saddle point-at-infinity ensures their uniqueness.

A transient slow (fast) one-dimensional manifold $\mathscr{W}$ is a finite-length invariant exponentially attracting manifold along which $r(\mathbf{z}) > 1$ ($r(\mathbf{z}) < 1$ for fast manifolds) for $\mathbf{z} \in \mathscr{W}$. Therefore, a transient manifold is not properly invariant, because $\phi_t(\mathscr{W}) \subset \mathscr{W}$ for $t > 0$, and $\lim_{t\to\infty}\phi_t(\mathscr{W}) = \mathbf{z}_{eq}$. This is the reason of the wording "transient" for this class of invariant geometric structures. Moreover, although proper invariant manifolds may be inverting, as extensively addressed in section 3 for the Semenov model, transient manifolds are, by definition, noninverting, and this is the reason their occurrence may be significant in the local behavior of a dynamical system close to the equilibrium point $\mathbf{z}_{eq}$ (see section 5).

Transient manifolds may originate from two distinct geometric/dynamical phenomena: either (i) they are connections between $\mathbf{z}_{eq}$ and a point on the boundary (such as $\mathscr{W}_t^f$ depicted in Figure 8), or (ii) they are local stable/unstable manifolds associated with the hyperbolic equilibrium point $\mathbf{z}_{eq}$, such as the finite-length slow manifolds occurring in the Semenov model for $\epsilon > \epsilon_c$, which are revealed by the coalescence of orbits as depicted in Figure 1C and Figure 8B. (It is important to stress once again that we are considering dynamical systems possessing a unique, globally attracting equilibrium point. More complex phenomenologies may arise for systems possessing multiple equilibrium points or stable oscillatory behaviors.)

In a two-dimensional system, a transient slow manifold close to $\mathbf{z}_{eq}$ is just a local slow manifold $\mathscr{W}^s_{\mathbf{z}_{eq},loc}$, which is tangent to the slow eigenspace at $\mathbf{z}_{eq}$. This kind of transient manifold can be referred to as the Hartman−Grobman manifold, due to the implications of the Hartman−Grobman theorem.[39] It is clear from the definition that the Hartman−Grobman slow manifold does not need to be unique, as there exists different ways of constructing them; certain conditions are maintained: (i) they are tangent to the slow eigenspace at the equilibrium point $\mathbf{z}_{eq}$, and (ii) they are noninverting.

A simple way for constructing the transient Hartman−Grobman slow manifold for the Semenov model is presented in Appendix B.

To sum up, local bifurcations at the point-at-infinity of the Pp-system provide a simple way for understanding the global behavior and the nature of the slow/fast invariant manifolds.

In the Semenov model for thermal explosions, a qualitative change in the manifold structure occurs as a consequence of a transcritical bifurcation at infinity. This bifurcation leads to the transition from a global slow manifold (defined for $\epsilon < \epsilon_c$) to a generalized slow manifold (for $\epsilon > \epsilon_c$) that close to $\mathbf{z}_{eq}$ is tangent to the fast eigenspace of the unique equilibrium point. In all those cases for which either a global slow manifold does not exist or still exists, it is characterized by inversion close to $\mathbf{z}_{eq}$; the local behavior close to the equilibrium point is controlled by the occurrence of a Hartman−Grobman slow manifold, which is a finite arc representing the geometric memory of the dynamical behavior prevailing close to $\mathbf{z}_{eq}$. In this case, the transient finite-length Hartman−Grobman may play an important role in connection with the application of model reduction methods, especially if one is interested in finite portions of the phase space close to the equilibrium, as discussed in section 5.2.

4.3. Other Models of Combustion Kinetics. The occurrence of local bifurcation at infinity modifying the structure of the invariant slow manifolds is not a peculiar property of the Semenov model, but it is present in other combustion and explosive systems. In the Semenov model, the transcritical bifurcation characterizing the slow-manifold structure is a consequence of the interplay between the Arrhenius monotonic and saturating behavior of the kinetic rate coefficients and the heat losses at the reactor walls. It is therefore highly plausible that similar local bifurcations at infinity may occur also for higher dimensional combustion systems characterized by an Arrhenius-type functional dependence of the rate coefficients on temperature. What is remarkable is that qualitatively similar features may occur for other, completely different models of combustion kinetics and explosions. This is the case of the classical chain-branching model for combustion and explosions

in isothermal conditions, which is characterized by a quadratic nonlinearity. This reflects into a quadratic nonlinearity in the associated Pp-system, and the Semenov model behaves at infinity as a linear system.

We analyze a simplified kinetic model usually adopted to illustrate how chain-branching systems may exhibit explosive behaviors.[30] Let R, P, and C be the reactant, the product, and the chain carrier, respectively. The initiation, propagation, and termination steps are, respectively, $R \rightarrow C$, $C + R \rightarrow P + \alpha C$, and $C \rightarrow P$, where α is the branching constant, equal to unity for straight-chain reactions.

By indicating with k_i, k_p, and k_t the rate constants of the three steps, we read the rate equations for the reactant and chain carrier as

$$\frac{dc_R}{d\tau} = -k_i c_R - k_p c_R c_C$$

$$\frac{dc_C}{d\tau} = k_i c_R + (\alpha - 1) k_p c_R c_C - k_t c_C \tag{24}$$

where c_R, c_C are molar concentrations. By introducing the following dimensionless variables and parameters $x = c_R/c_R^\circ$, $y = c_C k_p/k_i$, $t = k_i\tau$, $\epsilon = k_i/(k_p/c_R^\circ)$, and $\gamma = k_t/(k_p/c_R^\circ)$, where c_R° is a reference reactant concentration, one finds that the rate equations eq 24 attain the form

$$\frac{dx}{dt} = -x - xy = P_1(x,y) + P_2(x,y)$$

$$\frac{dy}{dt} = \epsilon^{-1}[x + (\alpha - 1)xy - \gamma y] = Q_1(x,y) + Q_2(x,y) \tag{25}$$

where $P_1(x,y) = -x$, $P_2(x,y) = -xy$, $Q_1(x,y) = \epsilon^{-1}(x - \gamma y)$, and $Q_2(x,y) = \epsilon^{-1}(\alpha - 1)xy$.

If ϵ is a small parameter (which physically means that the initiation is slower than the propagation step), the chain-branching model is readily expressed in a singularly perturbed form, where x and y are the slow and fast variables, respectively.

Let $\mathbf{z} = (x, y)$, so that eq 25 can be expressed in compact form as $d\mathbf{z}/dt = \mathbf{F}(\mathbf{z},\epsilon,\alpha)$. This system possesses a unique equilibrium point $\mathbf{z}_{eq} = (0, 0)$, and the eigenvalues of the Jacobian matrix at the equilibrium point $\mathbf{F}^*(\mathbf{z}_{eq},\epsilon,\alpha)$ are -1 and $-\gamma\epsilon^{-1}$. Provided that $\gamma\epsilon^{-1} \gg 1$ (henceforth, we consider exclusively this case), there is a significant time scale separation in the neighborhood of $\mathbf{z}_{eq}$. The eigenspace associated with the slow eigenvalue $\lambda^s = -1$ is given by $E^s_{\mathbf{z}_{eq}} = \{\mathbf{v} = (v_1, v_2) | v_1/v_2 = \gamma - \epsilon\}$, and the fast eigenspace (associated with $\lambda^f = -\gamma\epsilon^{-1}$) is $E^f_{\mathbf{z}_{eq}} = \{\mathbf{v} = (v_1, v_2) | v_1 = 0\}$. Therefore, system properties close to the equilibrium point $\mathbf{z}_{eq}$ are unaffected by the value of the branching constant α.

Throughout this paragraph, we set $\gamma = 2$ and let the other two parameters ϵ and α vary, keeping $\gamma\epsilon^{-1} > 10$, corresponding to more than 1 order of magnitude in the time scale separation at the equilibrium point.

It readily follows from eq 25 that $\mathscr{W}_y = \{(x, y) | x = 0\}$ is an invariant manifold of the system. It can be split into the two different invariant manifolds $\mathscr{W}_y^+ = \{(x, y) | x = 0, y \geq 0\}$ (in the physically admissible region) and $\mathscr{W}_y^- = \{(x, y) | x = 0, y \leq 0\}$.

By analysis of the behavior of the tangent and normal stretching rates along $\mathscr{W}_y^+$ (with the assumption $\gamma\epsilon^{-1} > 10$), it follows that

$$\omega_\tau(y) = -\gamma\epsilon^{-1} < 0 \qquad \omega_\nu(y) = -1 - y < 0$$

$$r(y) = \frac{1 + y}{\gamma\epsilon^{-1}} \tag{26}$$

$$\Lambda^\omega = \lim_{y \rightarrow 0} r(y) < 1 \qquad \Lambda^\alpha = \lim_{y \rightarrow \infty} r(y) > 1 \tag{27}$$

This implies that $\mathscr{W}_y^+$ is a properly invariant exponentially attracting generalized slow manifold tangent to the fast eigendirection at the equilibrium point $\mathbf{z}_{eq}$ for each value of the branching constant α. Conversely, the manifold $\mathscr{W}_y^-$ is linearly unstable because $\omega_\nu(y) = -1 - y > 0$ for $y < -1$.

A complete picture of the structure and properties of invariant manifolds can be obtained by analyzing the Pp-system associated with the chain-branching model. Equilibria at infinity for the $m = 2$ degree polynomial system eq 25 occur at the points $\mathbf{u}_{eq}^\infty = (u_1, u_2)$ on the equator of the Poincaré sphere $\partial\mathcal{S}_2^1$ and satisfy the equation

$$u_1 Q_2(u_1,u_2) - u_1 P_2(u_1,u_2) = u_1 u_2 [u_1(\alpha - 1)\epsilon^{-1} + u_2] = 0 \tag{28}$$

or, equivalently at polar angles θ and $\theta + \pi$, are solutions of the equation

$$G(\theta) = \cos\theta\, Q_2(\cos\theta,\sin\theta) - \sin\theta\, P_2(\cos\theta,\sin\theta)$$

$$= \cos\theta \sin\theta\, [(\alpha - 1)\epsilon^{-1} \cos\theta + \sin\theta] = 0 \tag{29}$$

Therefore, for $\alpha \neq 1$, the system eq 25 possesses six equilibrium points-at-infinity corresponding to polar angles $\theta_1^* = 0$, $\theta_2^* = \pi$, $\theta_3^* = \pi/2$, $\theta_4^* = 3\pi/2$, $\theta_4^* = \arctan(\delta)$, and $\theta_6^* = \arctan(\delta) + \pi$, where $\delta = (1 - \alpha)\epsilon^{-1}$.

The flow on $\partial\mathcal{S}_2^1$ is counterclockwise at points corresponding to polar angles θ where $G(\theta) > 0$ and is clockwise at points corresponding to polar angles θ where $G(\theta) < 0$. Equilibrium points-at-infinity and the flow on the equator of the Poincaré sphere $\partial\mathcal{S}_2^1$ are depicted in Figure 9 for the two different cases $\delta > 0$ (left panel) and $\delta < 0$ (right panel).

For $\delta > 0$ (i.e., $\alpha < 1$), points P_1 and P_3 are stable on $\partial\mathcal{S}_2^1$ (and are saddle nodes on the Poincaré circle $\mathcal{S}_2$), and P_5 is unstable on $\partial\mathcal{S}_2^1$ (and is an improper unstable node on $\mathcal{S}_2$). Because the chain-branching model is a second-degree polynomial system, the behavior of the Pp-system near the antipodal equilibrium points P_2, P_4, and P_6 is topologically equivalent to the behavior near P_1, P_3, and P_5, respectively, with reversed flow direction.

By decreasing the value of δ, we find that the point P_5 moves toward point P_1, it collapses on P_1 for $\delta = 0$, and for $\delta < 0$, P_5 moves into the fourth quadrant and becomes an unstable improper node. Correspondingly, for $\delta < 0$, point P_1 becomes unstable on $\partial\mathcal{S}_2^1$.

Therefore, by focusing on the dynamics restricted to $\partial\mathcal{S}_2^1$, we observe an exchange of stability between points P_5 and P_1, i.e, a transcritical bifurcation at the critical value of the parameter $\delta_c = 0$ (corresponding to $\alpha = 1$), as clearly shown in Figure 10 where the polar angles θ_5^* and θ_1^* of equilibrium points-at-infinity P_5 and P_1 and their stability (with respect to the flow on $\partial\mathcal{S}_2^1$) are shown as a function of the bifurcation parameter δ.

For the chain-branching model, as for the Semenov model, the occurrence of a transcritical bifurcation of the points-at-infinity determines the blow-up of the global slow manifold

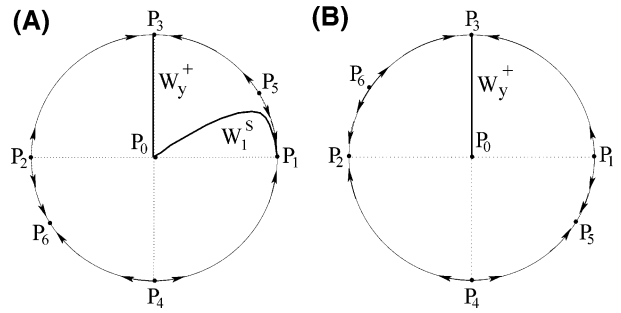

Figure 9. Critical points-at-infinity and flow on the equator of the Poincaré sphere $\partial\mathcal{J}_2^1$ for the system eq 25: (A) $\delta > 0$; (B) $\delta < 0$. Equilibrium points-at-infinity P_5 and P_6 correspond to polar angles $\theta_5^* = \arctan(\delta)$ and $\theta_6^* = \arctan(\delta) + \pi$. Bold curves $\mathcal{W}_1^s$ and $\mathcal{W}_y^+$ in the first quadrant represent the qualitative structure of the global and generalized slow manifolds, respectively.

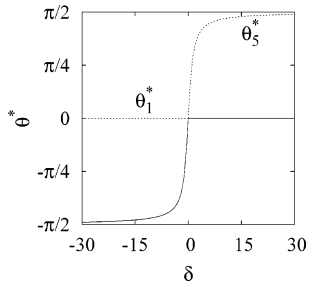

Figure 10. Polar angles θ_5^* and θ_1^* of points P_5 and P_1 and their stability (with respect to the flow on $\partial\mathcal{J}_2^1$) as a function of the bifurcation parameter δ: dotted line, unstable branch; continuous line, stable branch.

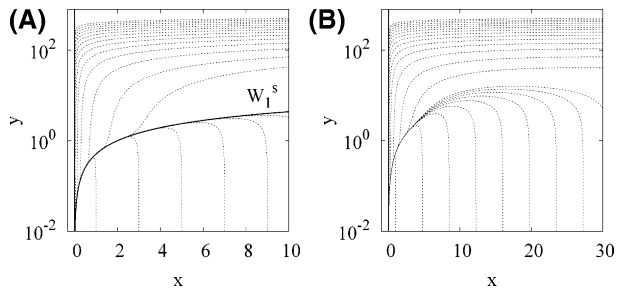

Figure 11. Phase-space diagrams of the chain-branching model in the x,y-plane ($x \geq 0$, $y \geq 0$): (A) $\gamma = 2$, $\epsilon = 5 \times 10^{-2}$, $\alpha = 0.95$, i.e., $\delta > 0$; (B) $\gamma = 2$, $\epsilon = 5 \times 10^{-2}$, $\alpha = 1.05$, i.e., $\delta < 0$. Dotted curves are phase-space orbits. Thick lines are global or generalized invariant manifolds.

$\mathcal{W}_1^s$ connecting the equilibrium point $\mathbf{z}_{eq}$ to the saddle node at infinity P_1 for $\delta > 0$.

This phenomenon can be appreciated from the analysis of Figure 11A,B showing the spatial behavior of phase-space orbits (dotted lines) and invariant manifolds (continuous lines) in the x,y-plane ($x > 0$, $y > 0$) for $\delta > 0$ (panel A) and for $\delta < 0$ (panel B). It can be observed that, for $\delta > 0$, the system possesses two coexisting (and in some sense competitive) slow manifolds: the generalized slow manifold $\mathcal{W}_y^+$ (connecting $\mathbf{z}_{eq}$ to the saddle node P_3, stable on $\partial\mathcal{J}_2^1$) and the global slow manifold $\mathcal{W}_{1s}$ (connecting $\mathbf{z}_{eq}$ to the saddle node P_1, stable on $\partial\mathcal{J}_2^1$) characterized by the ω/α-Lyapunov numbers $\Lambda^\omega = \gamma\epsilon^{-1} > 1$ and $\Lambda^\alpha = \infty > 1$.

For $\delta < 0$, the global slow manifold disappears and the spatial behavior of phase-space orbits is controlled by the still existing generalized slow manifold $\mathcal{W}_y^+$ and by the transient Hartman−Grobman slow manifold tangent to the slow eigendirection at the equilibrium point $\mathbf{z}_{eq}$.

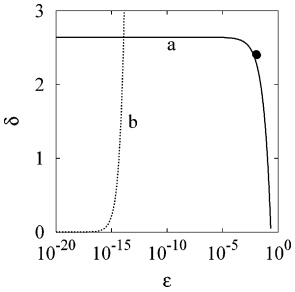

Figure 12. $\epsilon-\delta$ plot of the bifurcation/explosion loci for $\gamma = 1/\beta = 33$. Line a is the explosion limit according to the Adler−Enig criterion. Line b is the bifurcation locus. Dots (●) correspond to the experimental data by Gray et al. (ref 43) on the explosion limit for methyl nitrate decomposition.

To sum up, also for the chain-branching model, local bifurcations at the point-at-infinity of the Pp-system provide a simple way for understanding the global behavior and the nature of the slow invariant manifolds. As for the Semenov model, a qualitative change in the manifold structure occurs as a consequence of a transcritical bifurcation at infinity. This bifurcation leads to the transition from a global slow manifold (defined for $\delta > 0$ and coexisting with a generalized slow manifold) to a generalized slow manifold (for $\delta < 0$) that, close to $\mathbf{z}_{eq}$, is tangent to the fast eigenspace of the unique equilibrium point. Whenever a global slow manifold no longer exists, the local behavior close to the equilibrium point is controlled by a finite-length Hartman−Grobman slow manifold.

5. Explosions, Bifurcations, and Manifold Uniqueness

This section connects the analysis developed for the Semenov model with the experimental results on thermal combustion systems and on the occurrence of explosive behavior. Subsequently, the issue of slow manifold uniqueness and the implications of the results obtained for model simplification and reduction of kinetic schemes are critically examined.

5.1. Explosions. The Semenov model is widely known for being the paradigmatic example of explosive behavior in a closed, perfectly mixed system, in which the instability caused by an exothermic reaction is contrasted by the heat loss to the surrounding. In the classic 1928 article,[24] Semenov applied this model to present a simple bifurcational analysis of explosions grounded on the assumption of negligible reactant consumption, which holds for $\epsilon \to 0$.

Subsequently, several other authors have proposed different explosion criteria for the Semenov system eq 10 under generic operating conditions: Adler and Enig,[27] van Welsenaere-Froment,[42] Morbidelli and Varma,[28] just to quote some of the most representative. For a general analysis, see Varma et al. (1999).[29]

It is instructive to compare the experimental conditions typical of explosive dynamics with the parameter values leading to the transcritical bifurcation that modifies the structure and the properties of the slow manifolds.

Figure 12 shows the bifurcation locus of the transcritical bifurcations (curve b), and the explosion limit (curve a) for kinetic and operating conditions corresponding to the methyl nitrate decomposition studied by Gray et al. (1981).[43] The decomposition of the methyl nitrate (C_3ON_3) in the vapor phase is highly exothermic and can be treated as a first-order reaction. The heat of reaction at $T = 298$ K is given by $-\Delta H = 1.505 \times 10^5$ J/mol and may be assumed to be independent of temperature. Gray et al. performed experiments on a spherical reactor (radius (R) = 0.064 m, overall heat transfer coefficient

(U) = 3.0 J/(m^2 s K)), in the temperature range (T) 510−570 K, corresponding to a value of $\gamma = \beta^{-1} \simeq 33$ for different initial pressures.

The region below curve a in Figure 12 corresponds to explosive behavior for parameter values corresponding to the experimental data by Gray et al.;[43] the region on the right of curve b corresponds to operating conditions "after" the blow-up of the global slow manifold, where the system is characterized by a generalized slow manifold corresponding to the x-axis.

For the methyl nitrate decomposition, the experimental conditions by Gray et al. correspond to the occurrence of generalized slow manifolds, and this feature is generic for most of the simple explosive reactions that can be described by means of a first-order Semenov model (see, e.g., Varma et al. (1999)[29] for a survey of several experimental systems in this category). Specifically, in the case of azomethane ($(CH_3)_2N_2$) decomposition analyzed by Allen and Rice,[44] the dimensionless parameters for the reaction are $\gamma = 1/\beta = 39.8$, $\delta = 1.85$, and $\epsilon = 9.66 \times 10^{-3}$; for catalytic hydrolysis of acetic anhydride studied by Haldar and Rao,[45] $\gamma = 35.2$, $\delta = 1.4$, and $\epsilon = 7.46 \times 10^{-2}$. In both cases, $\epsilon > \epsilon_c$ and global dynamics are characterized by the occurrence of a generalized slow manifold (see Figure 1C,D for the phase-space portrait of the Semenov model in the presence of a generalized slow manifold). All the above observations indicate the physicochemical significance of the distinction between global and generalized manifolds and the genericity in the occurrence of the latter type of invariant structures in explosive reacting systems. This observation is further supported by the direct inspection of the phase portrait depicted in Figure 1 for the Semenov model. Whenever a global slow manifold exists (Figure 1A), the orbits converge smoothly toward the global manifold, and no explosive trajectories occur. The situation becomes slightly more unstable whenever a zone of inversion ($r(\mathbf{z}) < 1$) occurs (compare Figure 1B with Figure 1A); in contrast, sudden temperature variations, followed by a rapid and almost complete reaction consumption, typical of explosive conditions, characterize the presence of generalized slow manifolds (as depicted in Figure 1D).

Throughout this Article, the slow manifold structure and the dynamics within it have been characterized by means of the Lyapunov numbers Λ^{ω} and Λ^{α} eq 13 and ultimately on the comparison of tangential and normal stretching rates (e.g., the definition of the stretching ratio eq 14). It is intriguing to develop, within a unified formal apparatus, simple and consistent criteria for detecting explosion conditions and identifying the relevant explosion limits.

Following Thomas and Bowes[26] and Adler and Enig,[27] the explosive behavior can be regarded as the occurrence of a local accelerating behavior along system trajectories. Consequently, the occurrence of explosions can be viewed as a tangential instability, characterized by the fact that there exists a time $t > 0$ and a state $\mathbf{z}(t)$ along a system trajectory at which the tangential stretching rate ω_τ is positive as well as the integral of the tangential stretching rate,

$$\omega_\tau(\mathbf{z}(t)) > 0 \qquad \int_0^t \omega_\tau(\mathbf{z}(t'))\, dt' > 0 \qquad (30)$$

The latter condition expresses the property that, at time $t > 0$, $||\mathbf{F}(\mathbf{z}(t))|| > ||\mathbf{F}(\mathbf{z}(0))||$ (i.e., that the tangential dynamics is accelerating). This follows from the relation $||\mathbf{F}(\phi_t(\mathbf{z}))|| = ||\mathbf{F}(\mathbf{z})|| \exp(\int_0^t \omega_\tau(\mathbf{z}(t'))\, dt')$, which derives from eq 7. An increase of the norm of the vector field at some time instant t with respect to its initial value corresponds to a tangential acceleration.

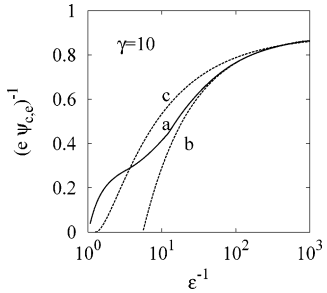

Figure 13. Explosion limit for the Semenov model at $\gamma = 1/\beta = 10$. Line a is the TSB criterion, line b the Adler−Enig criterion, and line c the van Welsenaere-Froment criterion. In this figure, $\psi = 1/\delta$.

The two conditions expressed by eq 30 can be viewed as the tangential-stretching-based (TSB) definition of potentially explosive conditions (referred to as runaway conditions) for the system. The locus in the parameter space at which these two conditions hold, at least for some time instant t, with the second replaced by an equality, defines the explosion limit according to the TSB approach.

Equation 30 can be applied in the case of generic reaction schemes. In the particular case of the Semenov model, eq 11, let $T(0) = T_c$ (i.e., the coolant temperature coincides with the initial reactant temperature, and let the reference concentration scale be equal to the initial reactant concentration). Under these assumptions, the initial conditions for eq 10 are $x(t=0) = 0$, $y(t=0) = 1$.

Figure 13 shows the comparison of the explosion limit for the Semenov system found according to the TSB approach and with two classical and widely used criteria for runaway: the criteria by Adler and Enig[27] and by van Welsenaere and Froment[42] for $\gamma = \beta^{-1} = 10$. The ordinate variable is the group ($e\psi_{c,e}$), where e = 2.718... is the Napier number and $\psi_{c,e}$ is the critical Semenov number (the group $\psi = \delta^{-1}$ is referred to as the Semenov number in the explosion literature).

The predictions of the TSB approach agree perfectly with the Adler−Enig criterion for $\epsilon^{-1} > 20$ and are qualitatively reasonable over the whole range of ϵ values. In fact, the region $\epsilon^{-1} > 4$ corresponds to operating conditions for which the assessment of the explosion limit displays some intrinsic problems, as also noted by Varma et al.[29] who resorted to parametric sensitivity analysis.

To sum up, the stretching analysis developed for manifold characterization provides simple, objective, and reliable criteria to assess the occurrence of explosive behavior in chemical systems. A thorough analysis of this issue and the application of the TSB criterion to complex kinetic schemes goes beyond the scope of this Article and is developed in a forthcoming work.

5.2. Manifold Nonuniqueness and Reduction Methods. The geometric characterization of manifold structure developed in sections 3 and 4 permits us to highlight some controversies and pathologies occurring in the application of model reduction methods for chemical systems.

Let us preliminarily observe that there is a conceptual difference between the geometric definition of slow invariant manifolds and the corresponding concept used in model reduction and kinetic diagnostics. This observation has been presented by Davis and Skodje[22] and can be further pinpointed by enforcing the concepts introduced above.

Following Davis and Skodje,[22] a (global/generalized) slow manifold is a heteroclinic connection between a stable equilibrium point and a saddle point-at-infinity. Conversely, in many engineering applications involving complex kinetic schemes, one is interested in finite portions of the phase space either

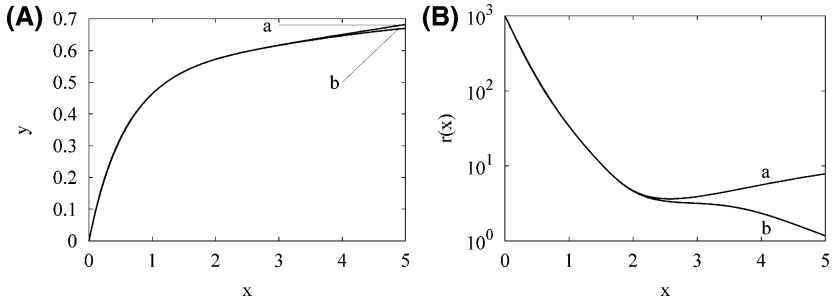

Figure 14. (A) Local normal hyperbolicity locus (shaded region) for the Semenov model for $\beta = 0.31$, $\epsilon = 10^{-3}$ in the region $0 \le x \le 5$, $0 \le y \le 1$. Curve a is the global slow manifold corresponding to the saddle node connection with a fixed point-at-infinity. Curve b is one of the infinitely many candidates for being a portion of an invariant exponentially attracting slow manifold in this region. (B) Stretching ratio $r(x)$ vs x along the two slow manifolds depicted in panel A.

because the physically admissible region is bounded or because the operating conditions of practical interest force the dynamics to be confined solely in specific regions of the phase space.

The main issue is the following: if one is interested in a finite-length slow manifold, by defining it under the conditions that (i) it is invariant for eq 1, (ii) it is exponentially attracting, and (iii) its normal perturbations decay faster than tangential ones, there are eventually infinitely many structures possessing these three properties.

To verify this statement via an example, consider the Semenov model and a bounded set $\mathscr{D}$ containing the equilibrium point, and define the set $\mathscr{D}_{\mathrm{LNH}} \subseteq \mathscr{D}$ as the set of points for which $\omega_\nu < 0$ and $\omega_\nu < \omega_\tau$. This set of points corresponds to the region in which the normal perturbations decay faster than tangential ones and correspondingly can be defined as the locus of local normal hyperbolic (LNH) behavior.

If one considers any initial condition belonging to $\mathscr{D}_{\mathrm{LNH}}$ such that the corresponding orbit is fully contained in the domain $\mathscr{D}_{\mathrm{LNH}}$, it follows from definition that any such orbit fulfills conditions i−iii stated above and therefore is a valid candidate for being considered as a "slow invariant manifold". For example, Figure 14A shows the local normal hyperbolicity locus for the Semenov model ($\beta = 0.31$, $\epsilon = 10^{-3}$), and lines (a) and (b) are two distinct forward orbits that may represent equally well a template for a slow invariant manifold in the bounded region $0 \le x \le 5$, $0 \le y \le 1$. The latter property can be confirmed by the behavior of the stretching ratio $r(x)$ vs x along these manifolds, which is depicted in Figure 14 panel B. This is a further indication of the intrinsic arbitrariness in the definition of slow manifolds in bounded domains of the phase space. In fact, the existence and the properties of the transient Hartman−Grobman manifolds are a further confirmation that global invariant structures (such as global/generalized slow manifolds) and local slow invariant manifolds with a stretching ratio greater than 1 may be, in some cases, two distinct and different point sets (e.g., Figure 17 panel E).

The classification of slow invariant manifolds using the dichotomies global/generalized inverting/noninverting can be used to frame some computational problems arising in connection with model reduction algorithms.

Indeed, global noninverting slow manifolds are the ideal invariant structure in view of achieving an efficient and reliable model reduction. Instead, the development of global inverting slow manifolds, that is, global slow manifolds along which the local stretching ratio $r(\mathbf{z})$ can, at least in a finite number of compact regions, take values lower than 1, i.e., where normal perturbations decay more slowly than tangential ones, affects model reduction in a number of ways.

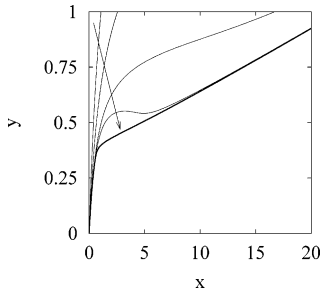

Figure 15. Convergence of the MLA method toward a global slow manifold for the Semenov model $\beta = 0.31$, $\epsilon = 10^{-2}$. The arrow indicates increasing times $t_n = 0.01, 0.02, 0.05, 0.1, 0.5$. The thicker line is the slow manifold.

First, as shown in section 3 with reference to the Semenov model, the region of inverting behavior causes the ILDM to be composed of two disconnected branches (Figure 3), the one emanating from the equilibrium point approximating the transient Hartman−Grobman manifold discussed in section 4.2 and the other branch approximating the other noninverting portion of the slow manifold.

Higher order methods such as the iterative methods by Roussel−Fraser (RF) or the computational singular perturbation (CSP) refinements are also unable to identify the global inverting slow manifold found by MLA, because these procedures either fail to converge or find multiple roots in the inverting region.

This implies that, whenever an inversion occurs, the diagnostic and reduction methods may perceive system dynamics as no longer one-dimensional and that normal modes should be necessarily accounted for. In other words, the phenomenon of stretching rate inversion along a global, and *a fortiori* a generalized slow manifold, explains why in the application of many model reduction algorithms (such as ILDM or CSP) a nonmonotonically decreasing variability in the number of active modes along system trajectories may be observed. This phenomenon can be fully appreciated in dynamical models in higher dimensional phase spaces than $n = 2$.

However, it is interesting to address the question of how the knowledge of the development of a global inverting slow manifold in a dynamical system, and the ability to identify it, can be related to model reduction.

By inspection of Figure 17 panel E, one can note that orbits starting on the y-axis, for small values of y, undergo a fast transient nearly parallel to the x-axis, and then they all coalesce onto the transient Hartman−Grobman manifold (thick solid line a); thus, this class of orbits is reducible along the transient Hartman−Grobman manifold as approached from small values of x.

However, for large values of y, all orbits turn around the extremum point of the Hartman−Grobman manifold (at $x =$

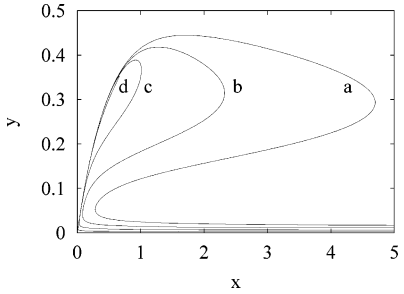

Figure 16. Semenov model for $\epsilon = 10^{-2} > \epsilon_c(\beta)$, $\beta = 0.21$. Convergence of material lines toward a generalized slow manifold. Plot of L_n for several values of t_n at the initial stages of the process. Line a refers to $t_1 = 0.1$, (b) to $t_2 = 0.12$, (c) to $t_3 = 0.15$, (d) to $t_4 = 0.2$. The initial material line L_0 coincides with the y-axis.

x*), are attracted by the noninverting portion of the global inverting slow manifold (labeled as (b) in Figure 17 panel E), and eventually are funneled along the global inverting slow manifold found by MLA (line b in Figure 17 panel E) until reaching the Hartman−Grobman manifold; thus, this class of orbits is reducible along the global inverting slow manifold, despite its inverting nature.

There exist two other types of dynamics corresponding to orbits with initial conditions either lying between the Hartman−Grobman manifold and the global slow manifold (line b) or below line b. In both cases, the orbits cross over the inverting region with paths nearly parallel to line b to eventually reach the Hartman−Grobman manifold; thus, these classes of orbits are also reducible along the Hartman−Grobman manifold as approached from large values of x.

This discussion points out that model reduction could indeed be possible even when a region of inversion occurs, but the reduced model cannot be expected to be built upon a single slow manifold constraint, because the development of the region of inversion induces a partitioning of the phase space in a number of basins of attraction characterized by requiring different low-dimensional manifolds as constraints. Clearly, although reasonably accurate approximations of the Hartman−Grobman manifold can be found by methods such as ILDM, CSP, and RF, none of these methods can identify the global inverting slow manifold, whereas, at least for one-dimensional manifolds, MLA has been demonstrated to be successful.

6. Concluding Remarks

This Article has developed a detailed analysis of the structure and the properties of slow manifolds in prototypical models of thermal combustion by focusing on the occurrence of local bifurcations (associated with the points-at-infinity) that modify the nature and existence of slow invariant manifolds.

The concept of slow invariant manifolds has been developed in a fully geometric framework divorced from any perturbative formulation. By making use of the Poincaré projected system,

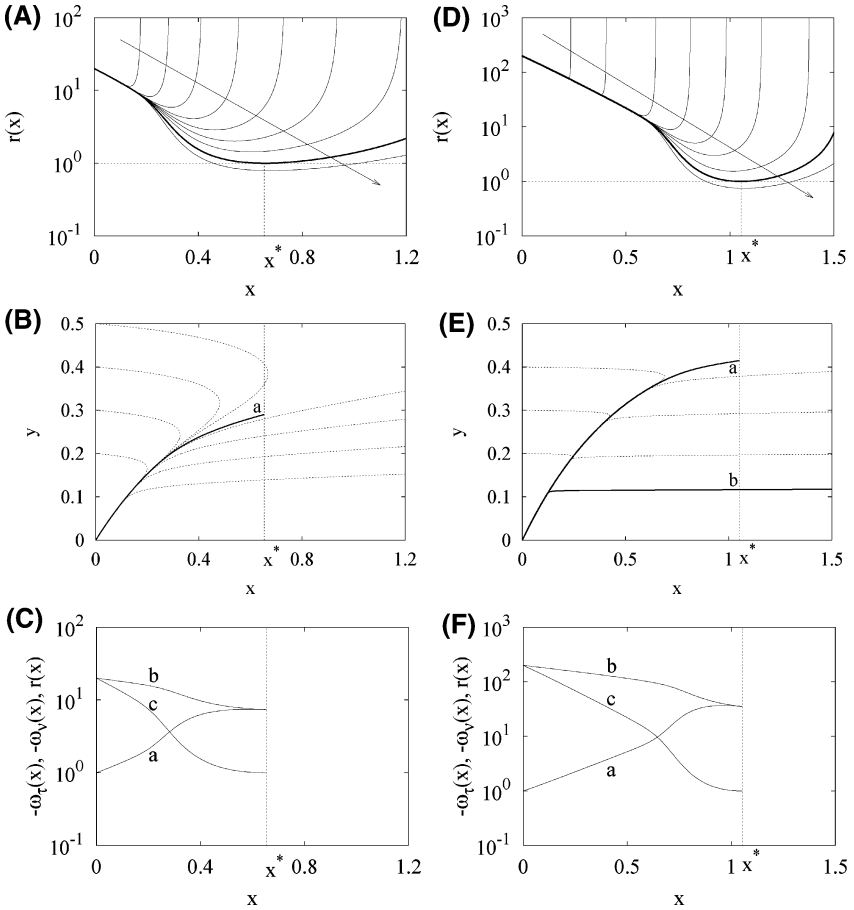

Figure 17. Estimate of the transient Hartman−Grobman slow manifold; $\beta = 0.31$ and $\epsilon = 5 \times 10^{-2} > \epsilon_c$ in panels A−C; $\beta = 0.21$ and $\epsilon = 5 \times 10^{-3} < \epsilon_c$ in panels D−F. (A) and (D) stretching ratio $r(x)$ vs x along different orbits starting on the y-axis for increasing values of y_0 (direction of the arrow). The dotted horizontal line is $r = 1$. The thick line shows the behavior of $r(x)$ along the particular orbit for which $r(x) \geq 1$ for $x \in [0, x^*]$, $r(x^*) = 1$, $dr(x)/dx|_{x^*} = 0$. (B) and (E) Transient Hartman−Grobman slow manifold and spatial behavior of nearby orbits (dotted lines). Curves a and b in (E) show the spatial behavior of the transient Hartman−Grobman manifold (line a) coexisting with the global slow manifold (line b). (C) and (F) Behavior of $-\omega_\tau(x)$ (curve a), $-\omega_\nu(x)$ (curve b), and $r(x)$ (curve c) vs x along the transient Hartman−Grobman slow manifold. The dotted vertical line indicates x^*.

a slow invariant manifold $\mathscr{W}$ can be viewed as the heteroclinic connection between the equilibrium point P_0 and the saddle point-at-infinity P_1. Material line advection provides a simple method to estimate $\mathscr{W}$.

Conversely, although the slow manifold so defined is unique, its dynamical properties may be "pathological" for what common sense expects to be a "well-behaved" slow manifold.

The occurrence and nature of the slow manifolds exhibited by a given dynamical system have a deep impact on the validity and the applicability of methods and techniques suited for model reduction and kinetic simplification. Although we considered in this Article solely low-dimensional prototypical models for combustion and explosions, the qualitative characterization of the invariant slow manifolds developed in section 3 provides useful and general hints on the computational difficulties that may be encountered in higher dimensional combustion models. Although in the presence of global slow manifolds it is expected that model reduction techniques may be successfully applied over the whole phase space, more complex situations may arise if solely a generalized slow manifold or a transient (Hartmann−Grobman) manifold exists. In the latter case, model reduction techniques may give rise to the detection of "apparent" slow manifolds that appear as disconnected sets (i.e., as a union of disconnected submanifolds) in which dimensional variability may occur (i.e., in which the number of slow variables may apparently be different within each disconnected submanifold). This phenomenon has been observed for high dimensional combustion systems and finds a clear interpretation within the geometric theory developed in this Article as a consequence of stretching-rate inversion (discussed in section 3.1). The extension of the geometric approach proposed in this article to kinetic schemes in phase spaces possessing dimensions higher than $n = 2$ is developed in ref 21.

Appendix A

The material line advection (MLA) technique is used in the analysis of fluid mixing systems to obtain the geometric structure of the invariant unstable manifolds.[35,36] The MLA technique for one-dimensional slow manifold identification is briefly reviewed below.

Given an infinite-length initial curve L_0 passing through $\mathbf{z}_{eq}$, consider the forward iterates $L_n = \phi_{t_n}(L_0)$, $n = 1, 2, ...$, where $\{t_n\}_{n=1}^{\infty}$ is a monotonically increasing sequence of positive time instants diverging to infinity.

For $n \rightarrow \infty$, L_n converges toward the global slow manifold, whenever it exists, or toward the generalized slow manifold.

In the practical implementation of the method, it is not necessary to consider "infinite-length" initial curves L_0 but solely a sufficiently long initial material line. Depending on the slowest fast time scale $\tau_{f,min}$ all over the phase space, it is sufficient to consider $t_n \in \mathscr{O}(\tau_{f,min})$ in order to achieve a satisfactory convergence toward an invariant slow manifold.

Figure 15 shows the convergence of the MLA method for the Semenov model at $\beta = 0.31 > \beta^*$ and $\epsilon = 10^{-2} < \epsilon_c$. The global slow manifold $\mathscr{W}^s$ is depicted with a thicker line. Observe that for $t_n = 0.5$ the material line already collapses onto $\mathscr{W}^s$.

The forward iterates of material lines allow the identification of local and generalized slow manifolds (which close to $\mathbf{z}_{eq}$ are tangent to the fast eigendirections). Figure 16 shows the evolution of a material line (initially coinciding with the nonnegative portion of the y-axis) at the early stages of the process for $\epsilon > \epsilon_c$.

As expected, at early times, material lines bend around a local slow manifold of the equilibrium point $\mathbf{z}_{eq}$ and progressively collapse toward the invariant manifold $\mathscr{W}^s_{1s}$ represented by the positive portion of the x-axis, which is the unique generalized slow manifold in the first quadrant.

Appendix B

In this appendix, we present a way for constructing the transient Hartman−Grobman slow manifold for the Semenov model. This can be performed by considering many different orbits starting from $(0, y_0)$ (i.e., points on the y-axis, $y_0 > 0$) for increasing values of y_0 and by analyzing the behavior of the stretching ratio r along the orbits. The Hartman−Grobman slow manifold can be defined as the maximal portion of the particular orbit of this family for which $r(x) \geq 1$ for $x \in [0, x^*]$ and such that $r(x^*) = 1$ and $dr(x)/dx|_{x^*} = 0$ (see Figure 17A, thicker line). The resulting transient manifold is depicted in Figure 17B together with the behavior of different orbits close to the equilibrium point $\mathbf{z}_{eq}$.

Figure 17C depicts the behavior of the tangential/normal stretching rates and of the stretching ratio along the transient manifold. It can be observed that $\omega_\nu(x) < 0$ and $\omega_\tau(x) < 0$ (i.e., the transient manifold is normally stable (exponentially attracting)) and $r(x) > 1$ (i.e., the transient manifold is a slow noninverting manifold).

The blow-up of a global slow manifold for $\epsilon > \epsilon_c$ makes the occurrence of transient Hartman−Grobman manifolds associated with the local behavior of the system close to $\mathbf{z}_{eq}$ particularly significant. However, the presence of such transient manifolds can be established also for $\epsilon < \epsilon_c$, in all the situations in which there exists a global slow manifold showing inversion close to $\mathbf{z}_{eq}$.

This phenomenon is depicted in Figure 17D−F for $\beta = 0.21$ and $\epsilon = 5 \times 10^{-3} < \epsilon_c$. In point of fact, Figure 17E shows the structure of the transient Hartman−Grobman manifold (line a) coexisting with the global slow manifold (line b) and the behavior of orbits close to the equilibrium point $\mathbf{z}_{eq}$. Visual inspection of Figure 17D−F indicates that the local behavior close to $\mathbf{z}_{eq}$ is essentially governed by the transient Hartman−Grobman manifold, although for the set of parameter values considered in Figure 17D−F, there exists a global (inverting) slow manifold.

References and Notes

(1) Griffiths, J. F. *Prog. Energy Combust. Sci.* **1995**, *21*, 25.
(2) Valorani, M.; Goussis, D. A. *J. Comput. Phys.* **2001**, *169*, 44.
(3) Hadjinicolau, M.; Goussis, D. A. *SIAM J. Sci. Comput.* **1999**, *20*, 781.
(4) Stephanopulos, G. N. *Metabolic Engineering: Principles and Applications*; Academic Press: New York, 1998.
(5) Kaznessis, Y. N. *Chem. Eng. Sci.* **2006**, *61*, 940.
(6) Maas, U.; Pope, S. B. *Combust. Flame* **1992**, *88*, 239.
(7) Lam, S. H. *Combust. Sci. Technol.* **1993**, *89*, 375.
(8) Lam, S. H.; Goussis, D. A. *Int J. Chem. Kinet.* **1994**, *26*, 461.
(9) Roussel, M. R. Fraser, S. J. *J. Chem. Phys.* **1990**, *93*, 1072.
(10) Eggels, R. L. G. M.; de Gooey, L. P. H. *Combust. Flame* **1995**, *100*, 559.
(11) Adrover, A.; Creta, F.; Giona, M.; Valorani, M.; Vitacolonna, V. *Physica D* **2006**, *213*, 121.
(12) Jones, C. K. R. T. in *Dynamical Systems*L. Arnold Ed.; Lecture Notes in Mathematics Vol. 1609, Springer-Verlag, Berlin, 1994.
(13) Kaper, H. G.; Kaper, T. J. *Physica D* **2002**, *165*, 66.
(14) Zagaris, A.; Kaper, H. G.; Kaper, T. J. *J. Nonlinear Sci.* **2004**, *14*, 59.
(15) Lorenz, E. N.; Krishnamurthy, V. *J. Atmos. Sci.* **1987**, *40*, 2940.
(16) Lorenz, E. N. *J. Atmos. Sci.* **1992**, *49*, 2449.
(17) Jacobs, S. J. *J. Atmos. Sci.* **1991**, *48*, 893.
(18) Goldfarb, I.; Goldshtein, V.; Maas, U. *IMA J. Appl. Math.* **2004**, *69*, 353.
(19) Hirsch, M. W.; Pugh, C. C.; Shub, M. *Invariant Manifolds*, *Lecture Notes in Mathematics*; Springer-Verlag: Berlin, 1977; Vol. 583.
(20) Gorban, A. N.; Karlin, I. V. *Chem. Eng. Sci.* **2003**, *58*, 4751.

(21) Giona, M.; Adrover, A.; Creta, F.; Valorani, V. *J. Phys. Chem. A* **2006**, 110, 13463.
(22) Davis, M. J.; Skodje, R. T. *J. Chem. Phys.* **1999**, *111*, 859.
(23) Davis, M. J.; Klippenstein, S. J. *J. Phys. Chem. A* **2002**, *106*, 5860.
(24) Semenov, N. N. *Z. Phys.* **1928**, *48*, 571.
(25) Semenov, N. N. *Some Problems of Chemical Kinetics and Reactivity*; Pergamon Press: London, 1999.
(26) Thomas, P. H.; Bowes, P. C. *Br. J. Appl. Phys.* **1961**, *12*, 222.
(27) Adler, J.; Enig, J. W. *Combust. Flame* **1964**, *8*, 97.
(28) Morbidelli, M.; Varma, A. *Chem. Eng. Sci.* **1988**, *43*, 91.
(29) Varma, A.; Morbidelli, M.; Wu, H. *Parametric Sensitivity in Chemical Systems*; Cambridge University Press: Cambridge, U.K., 1999.
(30) Williams, F. A. *Combustion Theory*; Addison-Wesley: Redwood City, CA, 1985.
(31) Sell, G. R.; You, T. *Dynamics of Evolutionary Equations*; Springer-Verlag: New York, 2002.
(32) Boothby, W. M. *An Introduction to Differentiable Manifolds and Riemannian Geometry*; Academic Press: Orlando, 1986.
(33) Wiggins, S. *Normally Hyperbolic Invariant Manifolds in Dynamical Systems*; Springer-Verlag: New York, 1994.
(34) Ryashko, L. B.; Shnol, E. E. *Nonlinearity* **2003**, *16*, 147.
(35) Alvarez, M. M.; Muzzio, F. J.; Cerbelli, S.; Adrover, A.; Giona, M. *Phys. Rev. Lett.* **1998**, *81*, 3395.
(36) Giona, M.; Adrover, A.; Muzzio, F. J.; Cerbelli, S.; Alvarez, M. M. *Physica D* **1999** *132*, 298.
(37) Roussel, M. R.; Fraser, S. J. *J. Phys. Chem.* **1993**, *97*, 8316.
(38) Fenichel, N. *Indiana University Math. J.* **1971**, *21*, 193.
(39) Irwin, M. C. *Smooth Dynamical Systems*; Academic Press: London, 1980.
(40) Perko, L. *Differential Equations and Dynamical Systems*, 2nd ed.; Springer-Verlag: New York, 1996.
(41) Kutznetsov, Y. A. *Elements of Applied Bifurcation Theory*, 2nd ed.; Springer-Verlag: New York, 1998.
(42) van Welsenaere, R. J.; Froment G. F. *Chem. Eng. Sci.* **1970**, *25*, 1503.
(43) Gray, P.; Griffiths, J. F.; Hasegawa, K. *Int. J. Chem. Kinet.* **1981**, *13*, 817.
(44) Allen, A. O.; Rice, O. K. *J. Am. Chem. Soc.* **1935**, *57*, 310.
(45) Haldar, R.; Rao, D. P. *Chem. Eng. Technol.* **1992**, *15*, 34.

(46) This note briefly reviews some concepts of dynamical system theory that will be used throughout the paper. Let $\mathscr{M}$ be an n-dimensional differentiable manifold, with $\mathscr{M} \subseteq \mathbb{R}^n$. A smooth curve through a point $p \in \mathscr{M}$ is a C^1-map γ: $(-a, a) \rightarrow \mathscr{M}$ with $\gamma(0) = p$. The tangent space to $\mathscr{M}$ at a point $p \in \mathscr{M}$, $T_p\mathscr{M}$, is the set of all vectors tangent to smooth curves passing through the point $p \in \mathscr{M}$. The tangent space $T_p\mathscr{M}$ is an n-dimensional linear space, and we shall view it as a subspace of $\mathbb{R}^n$. A vector field $\mathbf{f}$ on $\mathscr{M}$ is a function f: $\mathscr{M} \rightarrow \mathbb{R}^n$ such that $f(p) \in T_p\mathscr{M}$ for all $p \in \mathscr{M}$. If we define the tangent bundle of $\mathscr{M}$, $T\mathscr{M}$, as the disjoint union of the tangent spaces $T_p\mathscr{M}$ to $\mathscr{M}$ for $p \in \mathscr{M}$, then a vector field on $\mathscr{M}$ is a function f: $\mathscr{M} \rightarrow T_p\mathscr{M}$. Let us consider the system $\dot{\mathbf{x}} = f(\mathbf{x})$, where $\mathbf{x} \in \mathscr{M}$, with $\mathscr{M}$ being an n-dimensional manifold of class C^2 and $\mathbf{f}$ a C^1 vector field on $\mathscr{M}$. We have local existence and uniqueness of solutions through any point $x_0 \in \mathscr{M}$. A solution or integral curve on $\mathscr{M}$, $\phi_t(x_0)$ is tangent to the vector field $\mathbf{f}$ at x_0. If $\mathscr{M}$ is compact and $\mathbf{f}$ is a C^1 vector field on $\mathscr{M}$, then $\phi_t(x_0)$ is defined for all $t \in \mathbb{R}$ and $x_0 \in \mathscr{M}$, and it can be shown that (i) $\phi \in (\mathbb{R} \times \mathscr{M})$, (ii) $\phi_s^o\phi_t = \phi_{s+t}$ for any real values of s,t, where "$\circ$" indicates composition, i.e., $\phi_s^o\phi_t(\mathbf{p}) = \phi_s(\phi_t(\mathbf{p}))$. ϕ_t is called the phase flow on the manifold $\mathscr{M}$ associated with the vector field $\mathbf{f}$. By definition, $d\phi_t(\mathbf{x})/dt = f(\phi_t(\mathbf{x}))$. If the manifold $\mathscr{M}$ is the phase space $\mathbb{R}^n$ itself, we indicate the tangent space of $\mathbb{R}^n$ at $\mathbf{z}$ simply as $T_{\mathbf{z}}$.

(47) Let c and T be the concentration of the reactant A and the temperature, respectively. The energy and mass balance equations read

$$\rho\, c_v \frac{dT}{d\tau} = (-\Delta H) k_0 e^{-E/RT} c - Ua(T - T_c) \quad \frac{dc}{d\tau} = -k_0 e^{-E/RT} c$$

where τ is the physical time, ρ the density, c_v the specific heat, $(-\Delta H) > 0$ the reaction heat, k_0 the kinetic rate prefactor, E the activation energy, U the overall heat transfer coefficient, a the specific exchange surface area (i.e., the ratio of the heat exchange area to the reactor volume), and T_c the coolant temperature. By introducing the dimensionless variables, $x = (T - T_c)\gamma/T_c$, $y = c/c_0$, $t = \tau k_0 e^{-\gamma}$, where c_0 is a reference concentration value, $\gamma = E/RT_c$, $\beta = 1/\gamma$, $P = \gamma(-\Delta H)c_0/\rho c_v T_c$, $Q = Ua e^{\gamma}/\rho c_v k_0$, $\delta = Q/P$, $\epsilon = P^{-1}$, the dimensionless formulation of the Semenov equations attains the form of eq 10.

(48) If ϵ is a small parameter in the Semenov model, eq 10 is already expressed in a singularly perturbed canonical form and the reduced manifold $\mathscr{W}'_{red}$, defined for $\epsilon = 0$, reads as $\mathscr{W}'_{red} = \{(x, y) | y = h(x) = x\delta/q(x), x \in (x_c, \infty)\}$, where the value $x_c = -1/\beta$ corresponds physically to $T = 0$ K. It can be shown that, for $\beta > 1/4$, $\mathscr{W}'_{red}$ is linearly stable and the conditions of the Fenichel theorem apply, so that there exists, for sufficiently small ϵ, an invariant manifold $\mathscr{W}'_\epsilon$ that is $\mathscr{O}(\epsilon)$ close to $\mathscr{W}'_{red}$, and $\mathscr{W}'_{red}$ can be viewed as the slow-dynamic template at $\epsilon = 0$. For $\beta < 1/4$, $\mathscr{W}'_{red}$ is linearly unstable, and its nonmonotonic behavior (it exhibits a maximum and a minimum as a function of x) does not correspond to any limit template for the slow invariant manifold $\mathscr{W}'_\epsilon$ as $\epsilon \rightarrow 0$. This claim can be simply proved as follows. The one-dimensional slow manifold is an invariant manifold. Therefore, given a point $\mathbf{z}^* = (x^*, y^*)$ belonging to it, the phase flow $\phi_t(\mathbf{z}^*)$ for $t \geq 0$ coincides with the portion of the slow manifold defined for $x \in [0, x^*]$. However, the behavior of $y(t)$, along a trajectory of the Semenov system starting from a point with $y^* > 0$, is monotonically decreasing, independently of the values of ϵ. Actually, $dy/dt < 0$, for all t, x, and this corresponds to the fact that y represents the dimensionless concentration of an irreversibly consumed reactant in a batch system, so that it must necessarily decrease in time. Suppose that the representation $y = h_\epsilon(x)$ for the invariant manifold $\mathscr{W}'_\epsilon$ possesses a local minimum at $x = x_m$, and take $x^* > x_m$. There would exist a region of the manifold at which $dy/dt > 0$, which is impossible by the irreversibility of the reaction.

(49) Consider a generic manifold $\mathscr{W}'$ different from $\mathscr{W}'^s$ and $\mathscr{W}'^f$ and a point $\mathbf{z} \in \mathscr{W}'$, $\mathbf{z} \neq 0$. A vector $\mathbf{c}_0(\mathbf{z})$ tangent to $\mathscr{W}'$ at $\mathbf{z}$ can be expressed as $\mathbf{c}_0(\mathbf{z}) = c_s\mathbf{e}^s + c_f\mathbf{e}^f$, where $\mathbf{e}^s$ and $\mathbf{e}^f$ are the eigenvectors of the coefficient matrix, associated with the eigenvalues $-\lambda^s$ and $-\lambda^f$, respectively, and c_s, $c_f \neq 0$ are real numbers. $\mathbf{c}_0(\mathbf{z})$ is parallel to $\mathbf{F}(\mathbf{z})$. For $t > 0$, $\mathbf{c}_t(\mathbf{z}) = c_s e^{-\lambda^s t}\mathbf{e}^s + c_f e^{-\lambda^f t}\mathbf{e}^f = e^{-\lambda^s t}[c_s\mathbf{e}^s + \mathscr{O}(e^{-(\lambda^f - \lambda^s)t})]$, where $\mathscr{O}(x)$ is a quantity order of its argument x. It follows that $\lim_{t\rightarrow\infty} \log||\mathbf{c}_t(\mathbf{z})||/t = -\lambda^s$. A normal vector $\mathbf{n}_0(\mathbf{z})$ at $\mathbf{z}$ can be expressed as $\mathbf{n}_0 = n_s\mathbf{e}^s + n_f\mathbf{e}^f$, where n_s, n_f are different from 0, and such that $\mathbf{n}_0 \perp \mathbf{c}_0$. At time $t > 0$, $\phi_t^*(\mathbf{z})\mathbf{n}_0 = n_s e^{-\lambda^s t}\mathbf{e}^s + n_f e^{-\lambda^f t}\mathbf{e}^f$. The norm $||\Pi_{\phi_t(\mathbf{z})}[\phi_t^*(\mathbf{z})\mathbf{n}_0]||$ of the normal projection is simply the absolute value of the vector product (indicated with "$\times$") of $\phi_t^*(\mathbf{z})\mathbf{n}_0$ times the unit tangent vector $\mathbf{c}_t(\mathbf{z})/||\mathbf{c}_t(\mathbf{z})||$, i.e., $||\mathbf{n}_t|| = |(\phi_t^*(\mathbf{z})\mathbf{n}_0) \times \mathbf{c}_t(\mathbf{z})|/||\mathbf{c}_t(\mathbf{z})||$. After the expressions for the two vectors derived above are substituted, and after some elementary algebra, it follows that $||\mathbf{n}_t|| = Ce^{-\lambda^f t} + \mathscr{O}(e^{-(2\lambda^f - \lambda^s)t})$, where $C = |(n_s c_f - n_f c_s)(\mathbf{e}^s \times \mathbf{e}^f)| > 0$. Therefore, $\lim_{t\rightarrow\infty} \log||\mathbf{n}_t||/t = -\lambda^f$, and $\Lambda^\omega = \lim_{t\rightarrow\infty} \log||\mathbf{n}_t||/\log||\mathbf{c}_t|| = \lambda^f/\lambda^s$. For Λ^α, the same procedure can be repeated, with the only difference that $\mathbf{c}_{-t}(\mathbf{z}) = e^{\lambda^f t}[c_f\mathbf{e}^f + \mathscr{O}(e^{-(\lambda^f - \lambda^s)t})]$ with $t > 0$. Therefore, $\lim_{t\rightarrow\infty} \log||\mathbf{c}_{-t}(\mathbf{z})||/t = \lambda^f$, and $||\mathbf{n}_{-t}(\mathbf{z})|| = |(\phi_{-t}^*(\mathbf{z})\mathbf{n}_0) \times \mathbf{c}_{-t}(\mathbf{z})|/||\mathbf{c}_{-t}(\mathbf{z})|| \sim e^{\lambda^s t}$. It follows that $\Lambda^\alpha = \lim_{t\rightarrow\infty} \log||\mathbf{n}_{-t}||/\log||\mathbf{c}_{-t}|| = \lambda^s/\lambda^f$, which proves the third line in Table 1. The other results reviewed in Table 1 can be obtained in the same way, by simply observing that, for $\mathscr{W}'^s$, $\mathbf{c}_0 = \mathbf{e}^s$, and, for $\mathscr{W}'^f$, $\mathbf{c}_0 = \mathbf{e}^f$.